CR-152067

NOV 1977
RECEIVED
NASA STI FACILITY

OCKHEED

SSILES & SPACE COMPANY, INC. • SUNNYVALE, CALIFORNIA

S U B S I D I A R Y   O F   L O C K H E E D   A I R C R A F T   C O R P O R A T I O N

DUST PARTICLE VELOCITY MEASUREMENT

By   Leroy O. Thielman

October 1976

Distribution of this report is provided in the interest
of information exchange. Responsibility for the contents
resides in the author or organization that prepared it.

Prepared under Contract No. NAS2-9280 by

LOCKHEED MISSILES AND SPACE CO., INC.

Sunnyvale, California

for

AMES RESEARCH CENTER
NATIONAL AERONAUTICS AND SPACE ADMINISTRATION

FOREWORD

This final report was prepared by Lockheed Missiles and Space Co., Inc. under NASA Contract NAS2-9280 and covers work performed during the period June 1976 to November 1976. This work was administered under the direction of NASA Ames Research Center with William B. Van Ark as the technical monitor. The chief investigator was Dr. Leroy O. Thielman, with support from Dr. John S. Osmundson and Norman L. Thomas of LMSC. Acknowledgement is given to the valuable contributions made by Dr. F. C. Witteborn and Dr. L. S. Young of NASA/ARC.

ABSTRACT

Lockheed Missiles and Space Company developed and used a Laser Doppler
Velocimeter (LDV) to measure the velocity distributions for particles
entering a vacuum chamber from the atmosphere through calibrated leaks.
The relative number of particles per velocity interval was obtained for
particulates of three size distributions and two densities passing through
six different leak geometries. The velocity range 15 to 320 meters per
second was investigated. Peak particle velocities were found to occur
in the 15 to 150 meters per second range depending upon type of particle
and leak geometry. A small fraction of the particles were found to have
velocities in the 150 to 320 meters per second range.

LOCKHEED MISSILES & SPACE COMPANY, INC.

TABLE OF CONTENTS

Section 1

INTRODUCTION

The effect of contaminants on the Space Shuttle infrared telescope facility (SIRTF) depends on the velocity distribution of the contaminant particles with the degree of interference depending on the production rate, velocity and size of the particles. Leakage from pressurized equipment and from the manned areas of the Shuttle may be a primary source of particles with sufficient velocity to reach telescope fields of view. The size and the concentration of particles within such a volume can be based on postulates, and typical leak geometries can be simulated. It remains to measure the velocity of escaping particles because the velocity is very difficult to predict analytically.

This report contains a description of a Laser Doppler Velocimeter (LDV) developed to measure particle velocity distributions for four particle species and six leak geometries. Glass spheres with diameters of 13, 53, and 106 μm and polystryene with a 13μm diameter were used to, simulate Space Shuttle contaminants. The velocity range 15 to 320 m/s was investigated.

It was found that the distributions for smaller particles had peaks with peak velocities in the 15 to 150 m/s range. Larger particle distributions tended to not be peaked. Instead, these distributions were spread over a wide velocity range with decreasing numbers of particles at increasing velocities. The 106 μm diameter glass spheres had significant numbers in the 150 to 320 m/s range, while the 13 μm particles had very few in that range.

The following sections present LDV operating principles, the procedure used to measure velocity, a discussion of measurement accuracy and resolution of the LDV and finally, the data obtained and a discussion of the trends noted.

1-1

Section 2

THEORETICAL ANALYSIS OF MEASUREMENTS

The theory of operation for an LDV is presented in this section. First, it is shown that light scattered from moving particles is shifted in frequency from the incident light by an amount dependent upon the particle velocity and the scattering geometry. Then, it is shown how the amount of this frequency shift may be obtained by utilizing optical heterodyne detection. Finally, the optical arrangement is analyzed and a signal-to-noise ratio derived in terms of particle sizes and optical parameters.

2.1   Theory of Laser Doppler Velocimetry

This description of Laser Doppler Velocimetry (LDV) is based on the theory of optical-mixing spectroscopy.[1] Consider a monochromatic incident laser beam of frequency ω_i and wave vector $\vec{k}_i$. The electric field for this beam can be written

$$E_{inc}(t) = E_i \exp\left[-i(\omega_i t - \vec{k}_i \cdot \vec{r})\right]$$

where E_i is the amplitude of the electric field, and t and $\vec{r}$ denote time and position respectively. The light scattered from a particle at position $\vec{r}_p$ is given by

$$E_{sca}(t) = S\, E_{inc}(t)\, \frac{\exp\left[ik|\vec{R} - \vec{r}_p|\right]}{ik|\vec{R} - \vec{r}_p|}$$

---

(1) H. Z. Cummins and H. L. Swinney, Progress in Optics, Vol. III (North-Holland, Amsterdam, 1970), p. 135.

where k is the scattered wave number and S is the amplitude function which depends on the direction of the scattered light, the particle size and the particle's dielectric properties. If the scattered light is collected at $\vec{R}$ which is far from the scattering region, we can write $\left|\vec{R} - \vec{r}_p\right| \cong R$ and $k\left|\vec{R} - \vec{r}_p\right| \cong kR - \vec{k}_s \cdot \vec{r}_p$, where we have defined a scattered wave vector $\vec{k}_s = k\vec{R}/\left|\vec{R}\right|$. Therefore, the scattered electric field is

$$E_{sca}(t) = A \exp\left\{-i\left[\omega_i t + (\vec{k}_i - \vec{k}_s)\cdot\vec{r}_p\right]\right\}.$$

Here we have $A = SE_i \exp(ikR)/ikR$ being nearly a constant. Assuming the particle velocity does not change appreciably while crossing the scattering volume, we can write $\vec{r}_p(t) = \vec{r}_{po} + \vec{v}_p t$ where $\vec{v}_p$ is the velocity of the particle. The scattered electric field now becomes

$$E_{sca}(t) = A \exp\left\{-i\left[\omega_i t + (\vec{k}_i - \vec{k}_s)\cdot\vec{v}_p t + \phi_p\right]\right\}$$

where ϕ_p is a phase factor which depends upon the location of the scattering particle. We note that the optical frequency of the scattered light has been shifted in frequency

$$\omega_s = \omega_i + (\vec{k}_i - \vec{k}_s)\cdot\vec{v}_p.$$

Note also that this doppler shifter frequency is dependent upon the particle velocity and the scattering geometry.

The three optical arrangements [2] which differentiate between the three classes of LDV's are local oscillator heterodyne, symmetric heterodyne and differential heterodyne. We use the local oscillator heterodyne

(2) C. P. Wang, "A Unified Analysis on Laser Doppler Velocimeters", J. Phys. E, 5, 763 (1972).

arrangement as shown in Fig. 2-1. In this configuration, two parallel
laser beams of unequal intensity.are focused by a lens so that the two
beams intersect at the point of focus. This intersection defines the
scattering volume and the particles are incident from a direction normal
to the optical axis of the lens. Some of the light which is scattered
from the strong incident beam is in the direction of the weak reference
beam; both are recollimated by the second lens. The weak reference
beam and the scattered light are then focused upon an optical (square
law) detector at a remote location.

Beams of unequal intensity are used because the reference beam is limited
by the saturation power of the detector while the incident beam is only
limited by the available laser power. The output of the optical detector
is an AC signal whose frequency is the difference between the reference
frequency and the scattering frequency which is

$$f_D = (1/2\pi)(\vec{k}_i - \vec{k}_s)\cdot\vec{v}_p$$

Using $\left|\vec{k}_i\right| \cong \left|\vec{k}_s\right| = 2\pi/\lambda$, we see from Fig. 2-2 that the doppler shifted
frequency is

$$f_D = \frac{2v_p}{\lambda} \sin\theta$$

where λ is the wavelength in a vacuum.

To obtain two parallel laser beams, one being much less intense than
the other, an uncoated glass plate of thickness t and index of refraction
n is used. Referring to Fig. 2-3 and using Snell's law, we see that the
beam separation is given by

$$d = 2t \tan\theta_r \cos\theta_i$$

where $\theta_r = \sin^{-1}(1/n \sin\theta_i)$. The power reflection coefficient is

2-3

WEAK REFERENCE
BEAM

STRONG
INCIDENT
BEAM

d

$\vec{V}$

$\vec{k_i}$

θ

$\vec{k_S} + \vec{k}_{LO}$

POWER
DUMP

DETECTOR

F

F
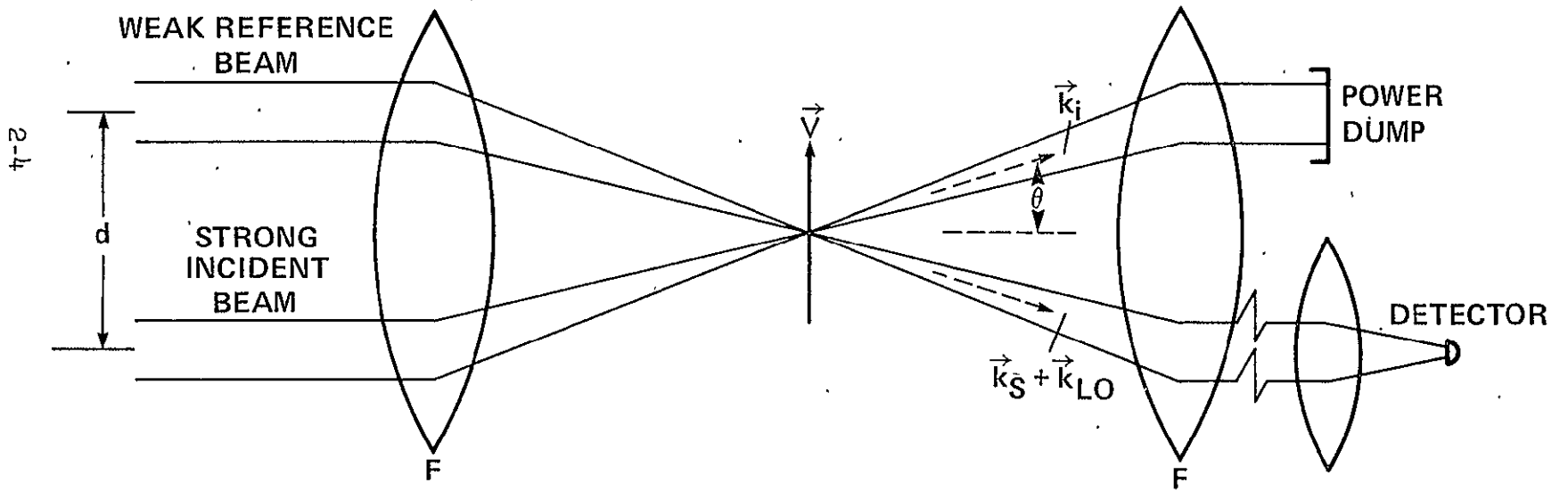
Fig. 2-1.   Local Oscillator Heterodyne Arrangement
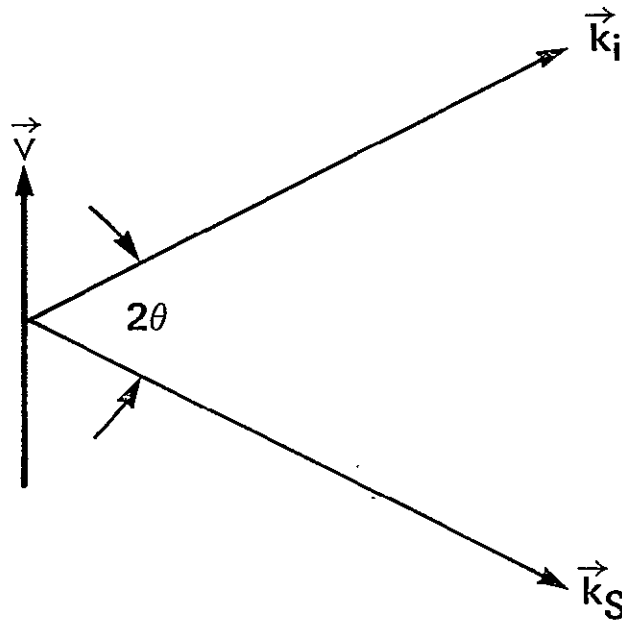
Fig. 2-2. Relation of Wave Vector to Velocity Vector

LOCKHEED MISSILES & SPACE COMPANY. INC.
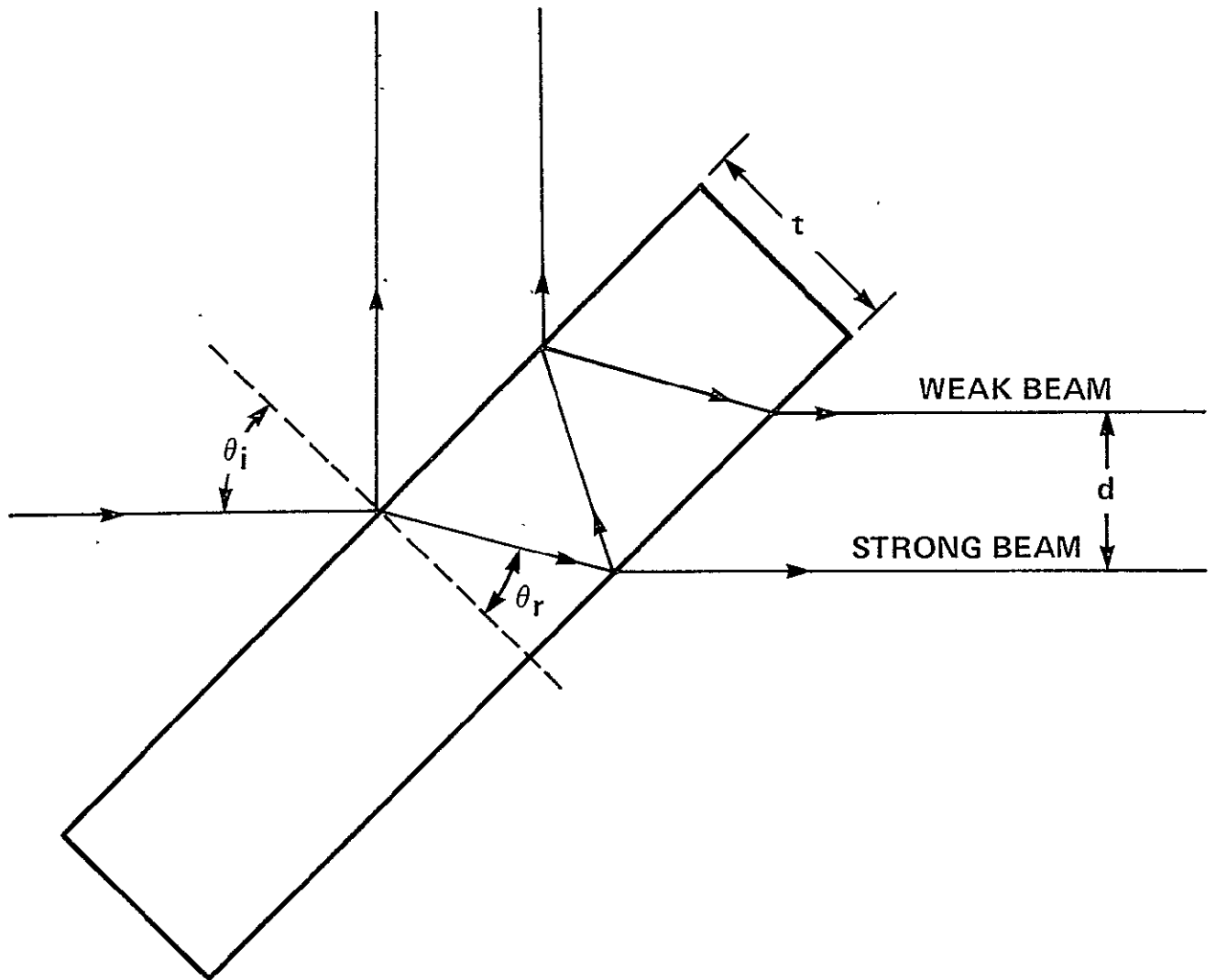
Fig. 2-3. Beamsplitter Used to Produce Two Parallel Beams

2-6

given by

$$R = \frac{\sin^2 (\theta_i - \theta_r)}{\sin^2 (\theta_i + \theta_r)}$$

If we assume an incident power P_i, then the power in the strong beam is $P_s = (1 - R)^2 P_i$ and the power in the weak beam is $P_W = R^2 (1 - R)^2 P_i$. Since $R \sim 1/10$, we see that the strong beam is about two orders of magnitude stronger than the weak beam.

2.2   Theory of Optical Heterodyne Detection

When two collinear optical beams are incident upon a detector, an AC signal at the difference frequency is obtained provided the frequency response of the detector is high enough. This can be seen in the following way. The electric field of the two optical beams is the sum of the electric field for each beam

$$E(t) = E_1 e^{-i\omega_1 t} + E_2 e^{-i\omega_2 t}.$$

The detector response is proportional to the square of this electric field

$$i(t) = \alpha \left\{ |E_1|^2 + |E_2|^2 + 2|E_1| \, |E_2| \cos \left[(\omega_2 - \omega_1) t + \phi \right] \right\}.$$

The first two terms are DC and can be removed with a blocking capacitor. The heterodyne signal current then is

$$i(t) = 2 \frac{e\eta}{\hbar\omega} \sqrt{P_1 P_2} \cos \left[(\omega_2 - \omega_1) t + \phi \right]$$

where e is the electronic charge, η is the detector quantum efficiency, $\hbar$ is Planck's constant divided by 2π, ω is the average optical angular frequency and P_i is the power in the ith optical beam.

2-7

Usually one optical beam is of very low intensity while the other can be made arbitrarily large (within the constraints of the optical detector). The high intensity beam is termed the local oscillator and designated by P_{LO}, ω_{LO}. The low intensity beam is the signal and is designated by P_s, ω_s.

There are two dominant sources of noise for the detector used. The first is detector Johnson noise and the second is shot noise due to the random arrival of photons in the local oscillator beam. The power signal-to-noise ratio (S/N) referred to the detector output is given by

$$S/N = \frac{2\left(\frac{e\eta}{\hbar\omega}\right)^2 P_{LO} P_s}{\left[\left(2e^2\eta/\hbar\omega\right)P_{LO} + \frac{4kTF}{R}\right] B}$$

Here k is Boltzmann's constant, T is the absolute temperature, F is the noise figure of the preamplifier, R is the value of the load resistor and B is the width of the bandpass filter. When P_{LO} is made large so that the first noise term dominates, the detection process is said to be quantum noise limited and the signal-to-noise ratio is given by

$$S/N = \frac{\eta P_s}{\hbar\omega B}$$

This limit is difficult to achieve in practice, but it can be approached reasonably closely.

When the local oscillator and signal beams are not exactly collinear, the detector response is degraded. The antenna theorem[3] applies which states that the area of the detector multiplied by the solid angle

---

(3) A. E. Siegman, "The Antenna Properties of Optical Heterodyne Receivers", Proc. IEEE, 54 1350 (1966).

field of view is on the order of the wavelength squared. For a circular detector of radius r, the half angle of the conical field of view is given by

$$\theta = \frac{\lambda}{\pi r}$$

Any signal power incident on the detector from outside this cone will not contribute to the signal current.

2.3   ANALYSIS OF OPTICAL BASELINE

In this section, we assume the output of the laser to be a TEM_{ooq} gaussian beam. The intensity distribution in a direction perpendicular to the direction of propagation for a gaussian beam is given by

$$I(r) = I_o e^{-8r^2/d_B^2}$$

where $r^2 = x^2 + y^2$, $I_o = 8P/\pi d_B^2$ is the on-axis intensity, and P is the total power of the beam. The beam diameter d_B increases with distance z along the direction of propagation according to

$$d_B = d_{B_o} \sqrt{1 + (2\lambda z/\pi d_{B_o}^2)^2} \ .$$

This is a hyperbolic distribution with d_{B_o} being the minimum beam diameter at the focus. For large z, the beam diameter expands in a conical shape with half angle $\theta = 2\lambda/\pi d_{B_o}$. Note that d_B is the $1/e^2$ intensity diameter.

We will make some simplifying assumptions to enable this analysis to proceed smoothly. First, when d_{B_o} is large, we will assume the beam has negligible expansion over the short distances involved in this work.

Second, when d_{B_σ} is small (as when a beam is focused by a lens), we will assume the beam expands linearly with distance with the half angle listed above.

The beam from the laser which is split into two beams and is incident on lens L_1 is large and, hence, will be assumed not to expand. The beams emerging from this lens are each focused to a diameter d_s. The half angle of the converging beam is given by $\theta = d_B/2F$ where d_B is the beam diameter at the lens. But the half angle is also given by $\theta = 2\lambda/\pi d_s$. Hence,

$$d_s = 4\lambda F/\pi d_B .$$

The intensity at the focus is given by

$$I(r) = 8P/\pi d_s^2 e^{-8r^2/d_s^2} .$$

The power incident upon a small particle in this beam is

$$P_p = \int_{area} I(r) dA$$

where the integral is over the cross sectional area of the particle. For a spherical particle of diameter d_p ($d_p \ll d_s$) on the axis of the focused laser beam, we have

$$P_p = 2d_p^2 P/d_s^2 .$$

The light incident upon the particle is scattered over 4π steradians by reflection, diffraction and refraction (if the particle is transparent) in a complicated angular distribution. Rather than calculate this angular distribution, we will assume all power incident on the particle is uniformly distributed over 4π steradians as from a point source. The solid angle subtended by the detector at the particle is

2-10

given by $\pi d_D^2/4F^2$ where d_D is the diameter of the detector. Hence, the scattered signal power which reaches the detector from a particle on the laser beam axis is given by

$$P_s = \frac{d_p^2 \, d_D^2 \, P}{8 \, d_s^2 \, F^2} \ .$$

In terms of the unfocused laser beam diameter d_B, the signal power is

$$P_s = \frac{\pi^2 \, d_p^2 \, d_B^2 \, d_D^2 \, P}{128 \, \lambda^2 \, F^4} \ .$$

The diameter of the detector is determined by the size of the iris in front of lens L_3. If $d_D > d_B$, then the area to which the heterodyne detector is sensitive is smaller than the incident illuminating laser beam and some of the laser power is wasted. If $d_D < d_B$, some of the local oscillator power is wasted. The optimum condition is when $d_D = d_B$. In this case, the signal power is given by

$$P_s = \frac{\pi^2 \, d_p^2 d_B^4 \, P}{128 \, \lambda^2 \, F^4} \ .$$

Note that this is only correct when the particle is on the laser beam axis. For other locations, less power is incident on the particle and, hence, less power is scattered into the detector. We can consider the value given as the peak signal power to be expected for a given scattering geometry. The peak heterodyne signal to noise ratio in the quantum noise limit then is

$$S/N = \frac{\eta}{\hbar \omega B} \ \frac{\pi^2 d_p^2 \, d_B^4 P}{128 \lambda^2 \, F^4} \ .$$

2-11

Using $\omega = 2\pi c / \lambda$, we have

$$S/N = \frac{\pi \eta \, d_p^2 d_B^4 p}{256 \hbar c \lambda F^4 B}$$

For the following typical values

$\eta \quad = \quad 0.5$

$d_p \quad = \quad 13 \, \mu m$

$d_B \quad = \quad 1.3 \, mm$

$\lambda \quad = \quad 514.5 \, nm$

$F \quad = \quad 30 \, cm$

$P \quad = \quad 320 \, mW$

$B \quad = \quad 100 \, kHz$

we have S/N = 48.6 dB. Experimentally, we measure a peak signal to noise ratio of 48 dB. Since we were not at the quantum noise limit, the closeness of the two values indicates that we were receiving more power than what would be expected from a uniform scatterer.

LOCKHEED MISSILES & SPACE COMPANY. INC.

Section 3
EXPERIMENTAL ARRANGEMENT

This section describes each element of the experimental arrangement and
includes the values of component parameters. In addition to the LDV,
the section covers the method of particle generation, scattering volume,
the signal processor, types of leak geometry, and the particles used to
simulate the dust contaminants. The system was designed so that all
active elements such as the laser, detector, and signal processor
were placed outside the vacuum chamber.

The particle generator was designed so that particles entered the vacuum
chamber and passed through the scattering volume in surges. The amount
of doppler frequency shift per unit velocity per particle was a factor
determined primarily by geometrical parameters. Therefore, by varying
these parameters, the data could be made to occur at convenient frequency
intervals, i.e., from 0.4 MHz to 10.0 MHz. The sensitivity of the LDV
in this interval was 32 m/s/MHz. As a particle passed through the scatter-
ing region, an RF pulse was generated in the optical detector. By
counting the number of pulses per frequency interval, the particle velocity
distribution could be obtained for a given particle size distribution and
for a given leak geometry.

3.1   Equipment Configuration

The experimental arrangement used is depicted in Fig. 3-1. Figs. 3-2
and 3-3 show the laser, laser beam path, and vacuum chamber. A Spectra
Physics Model 165 Argon-Ion laser equipped with prism end mirror and
air spaced etalon was used. The laser generated about 400 mW at
λ = 414.5 nm, in a single longitudinal cavity mode. The output amp-
litude was actively stabilized to within 1/2%.

3-1

PARTICLE
DISPENSER

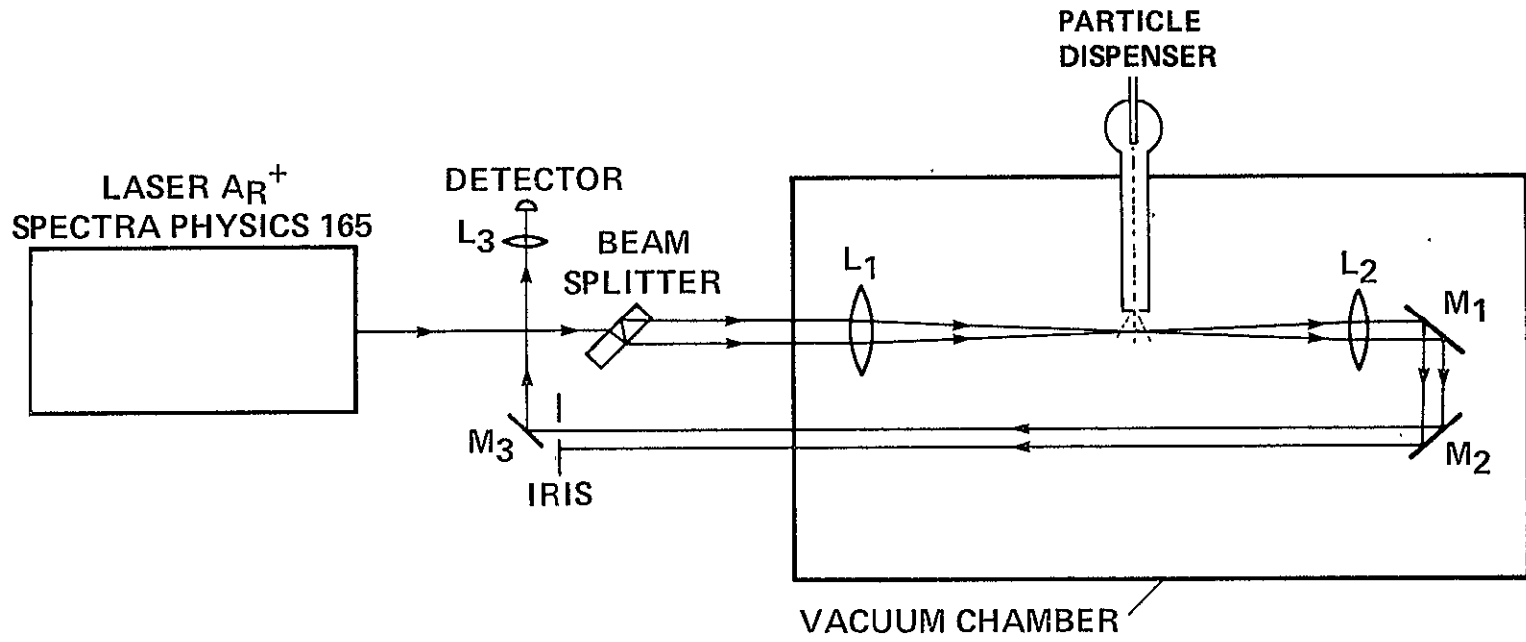LASER A$_R^+$
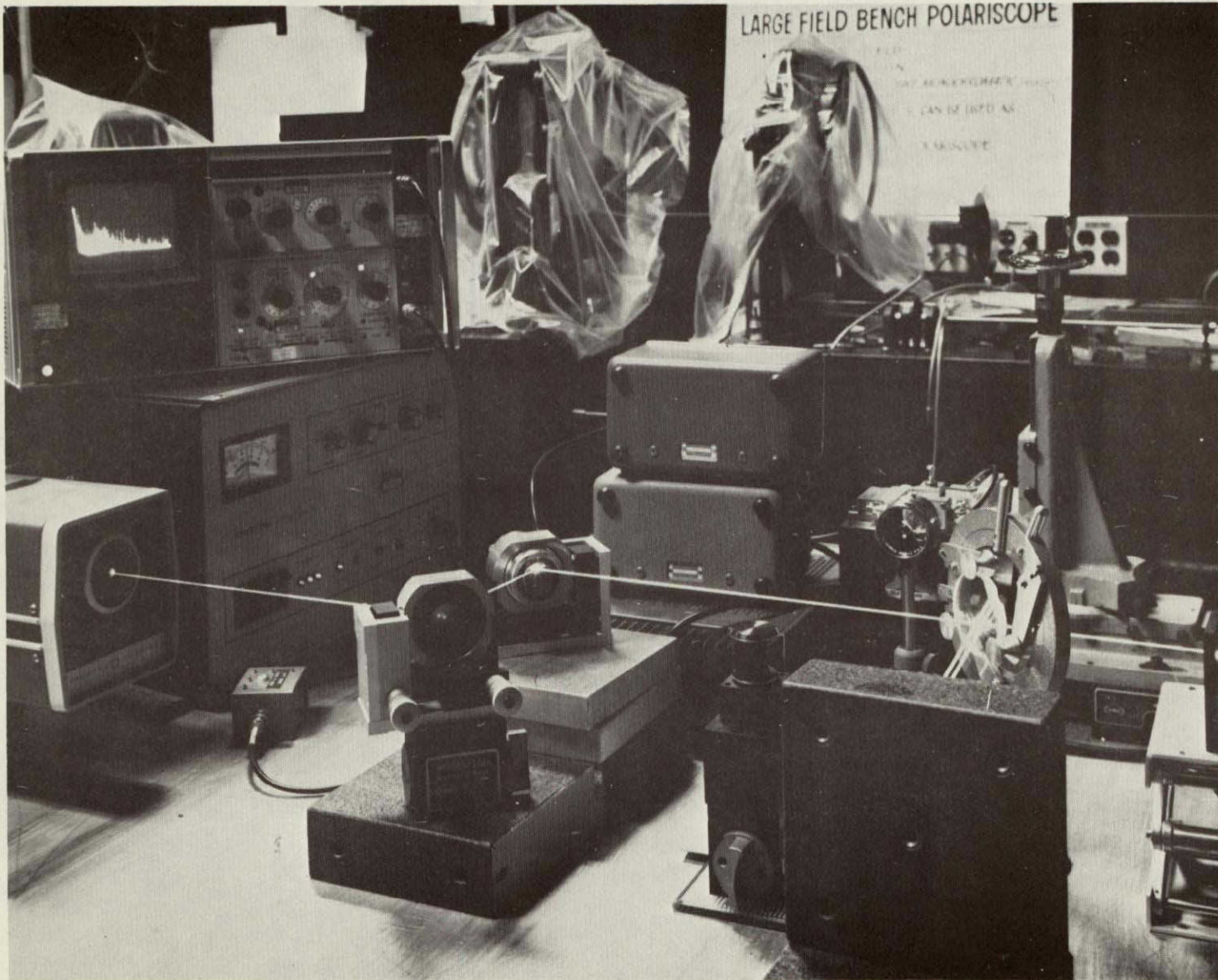SPECTRA PHYSICS 165

DETECTOR

L$_3$

BEAM
SPLITTER

L$_1$

L$_2$

M$_1$

M$_3$

M$_2$

IRIS

VACUUM CHAMBER

Fig. 3-1. Experimental Arrangement

3-3

LMSC/D-570053

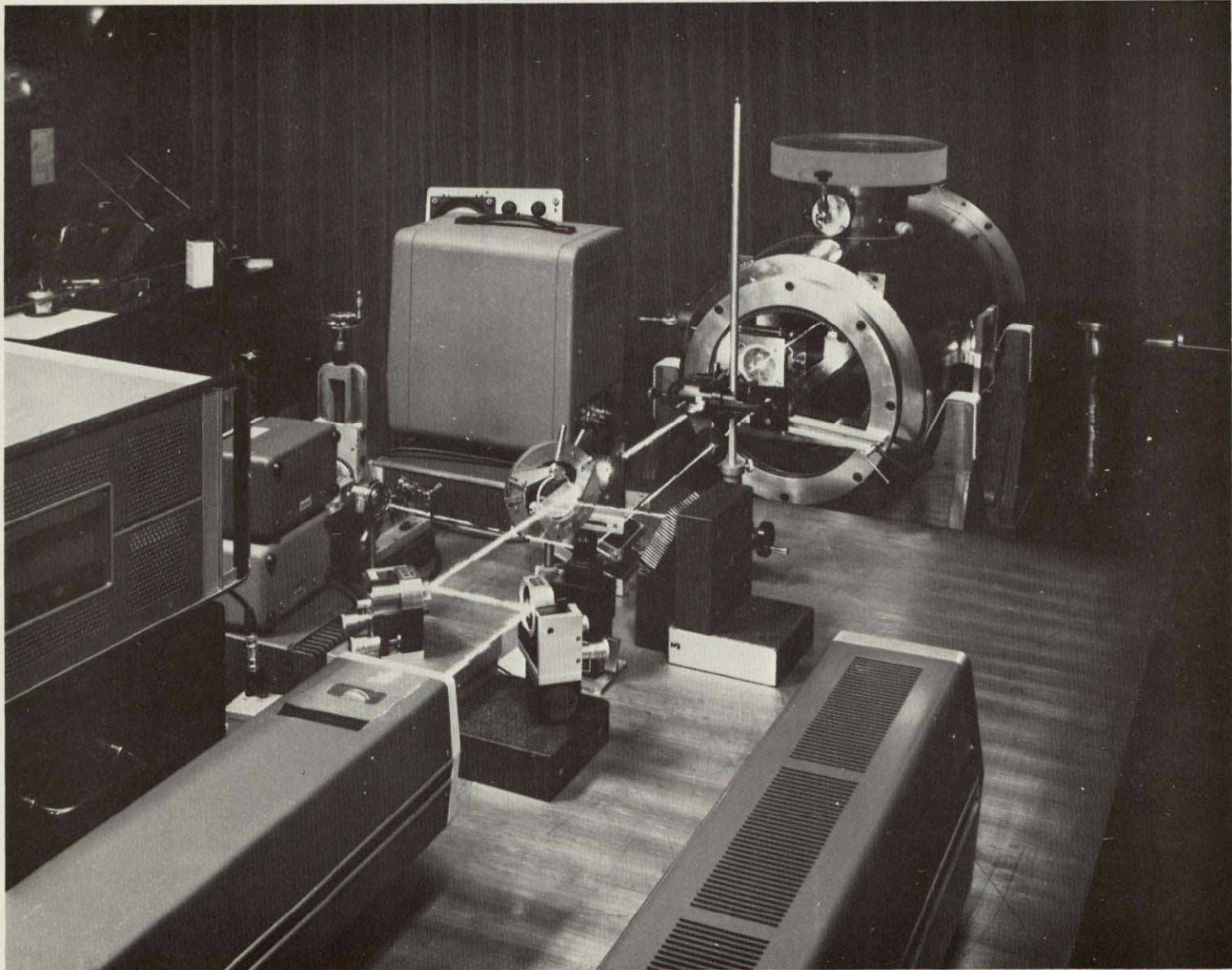Fig. 3-2. LDV and tunable filter

Fig. 3-3. LDV and Vacuum Chamber

The beam splitter was a glass plate 6.35 mm thick with an index of refraction of 1.5 which separated the two beams by 4.8 mm when oriented 45° from the incident beam. With this separation, the LDV sensitivity was 32 m/s/MHz. The reflection coefficient of the beam splitter at 45° is 9.2% and, hence, P_s = 330 mW and P_W = 2.8 mW. Although the power of the weak reference beam was not strong enough to operate the detector in the quantum noise limited condition, it maintained a sufficient S/N for this work.

The lenses L_1 and L_2 were both 30 cm focal length; in the final configuration, the strong beam was blocked before L_2 so as to reduce optical scattering from the following optical elements. This extraneous scattered light from the many optical elements was nearly as intense at the detector as the weak reference beam. This resulted in a doubling of the photon noise without an increase in signal. Lens L_3 was 5 cm focal length and focused all radiation passing through the iris onto the detector.

The detector used was a PIN photodiode HP5082-4220, reverse-biased at 10 V coupled to a Tron-Tech W200B preamplifier. With a multi-mode HeNe laser as a source, this is capable of detecting longitudinal cavity mode beat frequencies as high as 1.5 GHz. However, with the optical configuration used here, no data higher than 10 MHz was observed.

3.2   Particle Generation

The experiment was designed to simulate dust particles escaping from an atmospherically-pressured Space Shuttle cabin into the vacuum of outer space. The large diameter of leaks used ($\cong$ 350 μm) to enable large quantities of particles to reach the scattering volume made it difficult to maintain a good vacuum. The steady state vacuum with mechanical pumping was about 0.5 Torr. This was felt to be low enough since most of the acceleration given to a particle occurs across the 759.5 Torr

differential, and very little across the remaining 0.5 Torr differ-
ential. The particle generator is shown in Fig. 3-4. The glass portion
consists of a particle reservoir with a narrow air inlet near a constrict-
ion. The large opening is connected by vacuum tubing to the long hollow
aluminum cylinder. The vacuum "leaks" were drilled in a brass plate,
soldered to copper tubing and attached with "SwageLok" fittings to the
aluminum cylinder which fits into a vacuum quick-connect so that the
entire apparatus can easily be removed from the vacuum chamber.

As there was insufficient air flow through the particle generator to
sweep up particles from the reservoir and drive them through the leak
into the vacuum chamber, the air inlet to the particle generator was
blocked for about 15 seconds and then unblocked. The surge of air then
picked up the particles and carried them through the leak.

3.3 Scattering Volume

The scattering volume is defined by the intersection of the strong
incident and weak reference laser beams as shown in Fig. 3-5. If the
diameter of the two beams at the intersection is given by d_s and the
intersected angle is 2θ , then the length of the scattering volume L
is given by

$$L = \frac{2d_s \cos\theta}{\sin^2\theta}$$

and the maximum width by

$$w = \frac{2d_s \sin\theta}{\sin^2\theta} \quad .$$

With d_s = 200 μm and θ = 8 mrad, then L = 25 mm and w = 200 μm.
Actually, the effective scattering volume is shorter than the L given
above for two reasons: (1) at the extreme edge, the strong incident

3-6

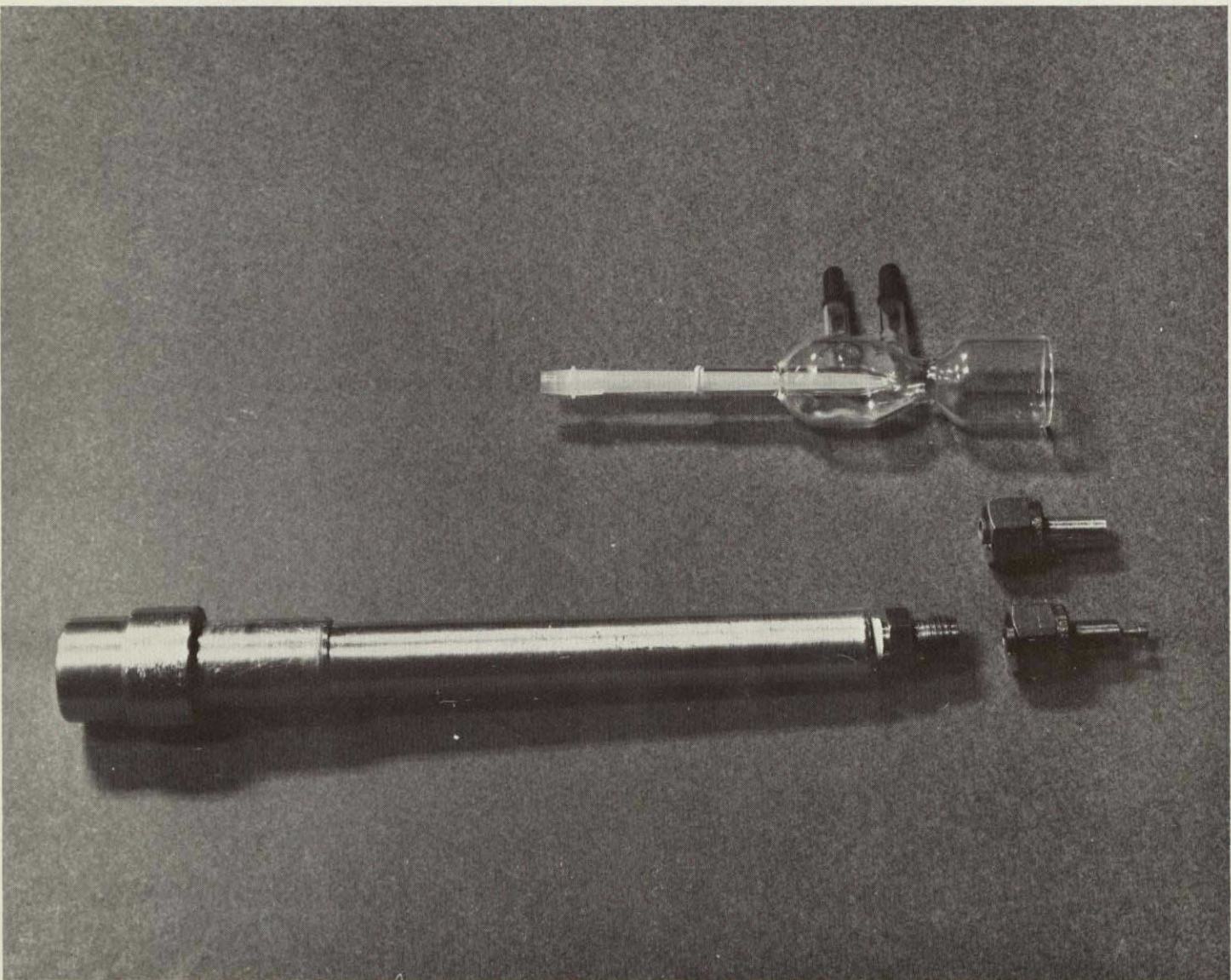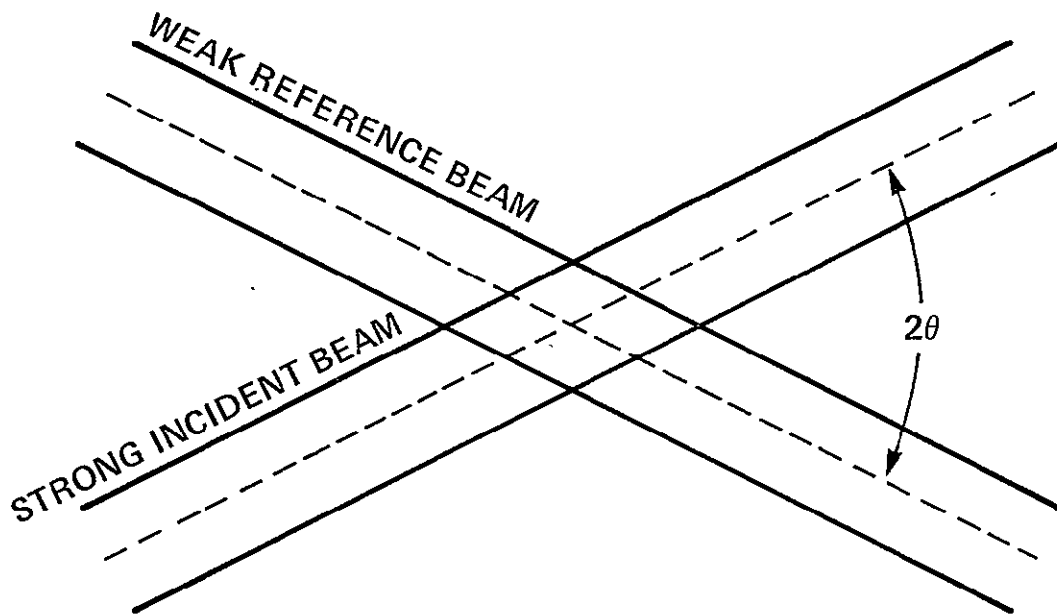Fig. 3-4. Particle Generator

Fig. 3-5. Scattering Volume

LOCKHEED MISSILES & SPACE COMPANY, INC.

beam intensity drops to $1/e^2$ (14%) of its on-axis intensity which drops the signal to noise ratio by 8.7 dB and, (2) the particle traverses this region so fast that very little RF energy passes through the electrical bandpass filter. As a compromise, we used L = 12.5 mm as the effective length of the scattering volume.

3.4   Signal Processing

As each particle passed through the scattering volume, an RF pulse whose center frequency was the doppler shifted frequency was detected. Pulse length varied between 1 and 100 μsec depending upon the speed of the particle and where it traversed the scattering volume. To obtain a distribution of particle velocities, the number of particles per frequency interval was obtained, as follows.

The signal at the preamplifier output was divided into two channels. One contained a bandpass filter with a fixed center frequency of 1.75 MHz and a bandwidth of 1 MHz. The other contained a variable center frequency bandpass filter variable from 0.4 to 10 MHz which corresponds to a range of velocities from 13 to 320 m/s. Although the bandwidth of the fixed filter could be varied, most data was taken with a bandwidth of 30 kHz.

After passing through the two filters, the RF pulses were then electronically detected, converted into DC pulses, and sent to an electronic counter. The pulses counted in both channels for each surge was tabulated. The fixed channel count was assumed to be proportional to the total number of particles dispensed in a given surge. After each surge, the center frequency of the variable filter was reset to another value and the counters reset to zero. This procedure continued until the entire frequency range of interest was covered. The ratio of the number of pulses counted in the variable channel to the number of pulses counted in the fixed channel for each variable channel center frequency

3-9

gave the particle velocity distribution.

3.5   Leak Geometry

The characteristics of the six leaks investigated in this study are summarized in Table 3-1:

Table 3-1: Simulated Leak Geometry

Leak Number	Orifice Diameter	Wall Thickness	General Description
1	200 μm	250 μm	Short cylindrical orifice
2	343 μm	125 μm	Short cylindrical orifice
3	343 μm	3.2 mm	Long cylindrical orifice
4	NC 2-56	3.6 mm (corresponds to about 8 threads)	Threaded orifice w/bolt inserted 4 turns; bolt head on atmospheric pressure side of wall; bolt diameter reduced by about 50 μm to facilitate particle flow.
5a	343 μm	343 μm	High pressure side of double walled leak, walls spaced 2.4 mm apart.
5b	1 mm	3.5 mm	Low pressure side
6a	343 μm	343 μm	High pressure side of double walled leak, walls spaced 2.4 mm apart.
6b	1.6 mm	3.5 mm	Low pressure side

The two cylindrical orifices in Leaks 5 and 6 were offset so that there was no optical path through them.

3.6   Particles

Glass spheres to simulate contaminants were obtained from the Micro-beads Division of Ferro Corporation, Jackson, Miss. Three sizes were used: the smallest with 80% in the 10-15 μm diameter range, the next with 85% in the 44-62 μm diameter range and the largest with 85% in the 88-125 μm diameter range. Polystyrene spheres were obtained from Royco in Menlo Park. These were mostly in a 2 μm range centered at 13 μm.

Chapter 4

ANALYSIS OF VELOCITY MEASUREMENTS

This section describes the accuracy of the velocity measurements and
the resolution of the LDV. Where all particles pass through the
scattering volume at the same speed, the response of the LDV is then
a broad peak, whose center is the particle speed. Anything causing
this center point to change contributes to measurement inaccuracy;
anything which broadens the peak degrades the system resolution.

Measurement inaccuracies are due to the uncertainties in measuring the
angle between the strong incident and the weak reference beams, and in
measuring the center frequency of the RF pulse generated for each particle.
The LDV's resolution is degraded due to the broad frequency content of
the short RF pulses and due to particles passing through the scattering
region in unanticipated directions. LDV measurement accuracy varies
between 10.5% to 20% depending upon velocity; its resolution is 14%.

4.1   Velocity Measurement Accuracy

The scattered light incident on the detector is doppler shifted by

$$f_d = \frac{2v}{\lambda} \sin \theta \ .$$

For small angles, the velocity is determined from

$$v = \frac{\lambda f_d}{2 \theta} \ .$$

4-1

The fractional accuracy of the velocity measurement is given by

$$\frac{\Delta v}{v} = \frac{\Delta \lambda}{\lambda} + \frac{\Delta \theta}{\theta} + \frac{\Delta f_d}{f_d} .$$

The uncertainty in laser wavelength measurement is determined by in-homogenous broadening of the Argon-Ion transition responsible for lasing. As this broadening is quite small ($\Delta\lambda/\lambda = 10^{-6}$), it is neglected hence-forth. The angle θ is given by half the separation between the weak re-ference beam and the strong incident beam divided by the focal length of the focusing lens. The fractional uncertainty in this angle is shown as:

$$\frac{\Delta \theta}{\theta} = \frac{\Delta d}{d}$$

The 4.8 mm distance can be measured to an accuracy of ±0.25 mm by simply measuring the center to center distance between the two beams, thus, $\Delta d/d = 0.10$. The uncertainty in measuring the doppler frequency depends on the accuracy of the variable filter, presently taken to be 30 kHz, (regardless of the center frequency). The doppler frequencies measured in this work ranged from 0.5 MHz to 10 MHz; thus, the maximum fractional uncertainty in measuring doppler frequency is 10%. Velocity measurement accuracies range from 20% at the lowest speeds to 10.5% at the highest.

4.2   Velocity Measurement Resolution

Three factors are involved in the resolution of the LDV. The first is due to the finite length of the scattering volume and the fact that particles escape from the leak orifice at all angles. If a particle passes through the scattering volume at an angle ϕ from the expected direction, the scattered light will be doppler shifted by an amount

4-2

$$f_d = \frac{2v \sin\theta}{\lambda} \cos\phi \quad .$$

The maximum value of ϕ is given by the scattering volume length divided by twice the distance from the orifice to the scattering volume. This angle was measured to be about 10°. The spread in velocity due to this effect then is

$$\delta v = \frac{\lambda f_d}{2\sin\theta} - \frac{\lambda f_d}{2\sin\theta \cos\phi} = v(1 - 1/\cos\phi).$$

which gives $\delta v/v = 1.5\%$.

The second factor is due to the changing value of θ as a particle traverses the scattering volume. This angle changes by an amount equal to the width of the scattering volume divided by the lens focal length. This value is about $\delta\theta/\theta = 4.2\%$ for a 200 μm scattering volume width.

The third factor bearing upon LDV resolution is the broad frequency content of the RF signal pulse from the heterodyne detector. A particle traverses the scattering region in a time $T = d_s/v$. The frequency spread of the induced RF pulse then is $\delta f = 1/2T = v/2d_s$. The fractional uncertainty in frequency then is

$$\frac{\delta f}{f} = \frac{v}{2d_s} \cdot \frac{\lambda}{2v\theta} = \frac{\lambda}{4d_s\theta} \quad .$$

For $d_s = 200 \mu$m and $\theta = 8$ m radians, we have $\delta f/f = 8\%$, so the total fractional velocity measurement resolution is

$$\frac{\delta v}{v} \cong 14\%.$$

LOCKHEED MISSILES & SPACE COMPANY, INC.

Chapter 5

RESULTS AND DISCUSSION OF DATA

Four variables were investigated under this contract: orifice diameter, orifice length, particle diameter, and particle mass density. In addition, special effects were noted with a double walled leak and a threaded orifice with a bolt inserted. The differences noted as these variables were varied independently were the velocities attained and the shape of the velocity distribution curves.

5.1 Orifice Diameter

Two orifice diameters were investigated with the 10 - 15 μm glass spheres. The first orifice was 200 μm diameter in a 250 μm thick wall, while the second was 343 μm diameter in a 125 μm thick wall. As indicated in Figs. 5-1 and 5-2, there did not appear to be any significant difference in the data for these two diameters. In both cases, there is a well defined velocity peak centered on 40 m/s with a width of about 38 m/s. While it would be better to have both wall thicknesses the same, the researchers felt that it is unlikely there could have been two effects here which were almost exactly cancelled.

5.2 Orifice Length

Two orifices with identical diameters of 343 μm in walls of differing thicknesses (125 μm and 3.2 mm) were next investigated with four different particle species. For each species, the same effect was noted, namely, the longer the orifice, the faster the particles moved. Figs. 5-2 and 5-3 show that the velocity peak for 10 - 15 μm glass spheres increases from 40 m/s to 96 m/s as the length of the orifice increases. The results also show a change in the velocity distribution
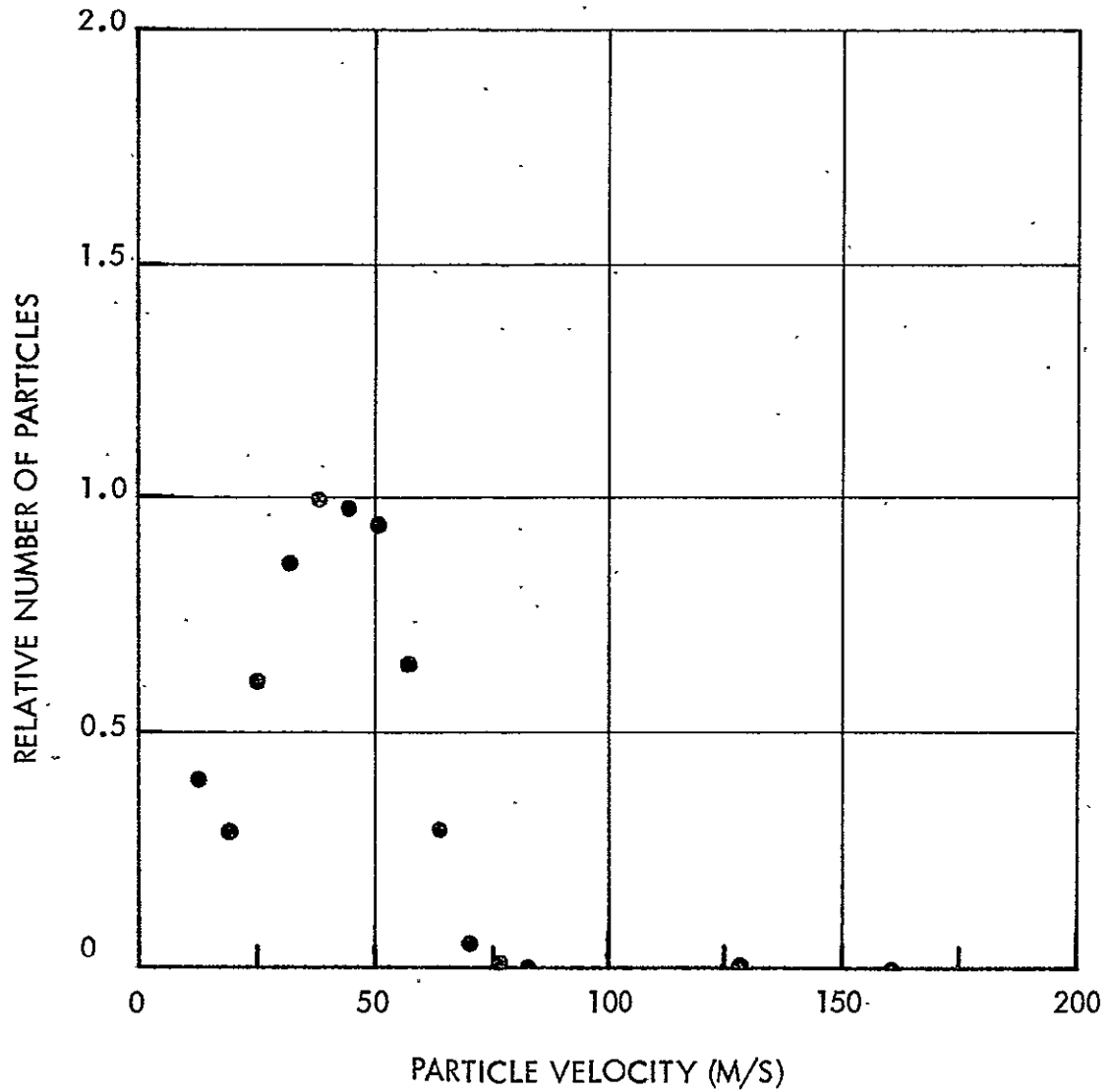
5-1

LOCKHEED MISSILES & SPACE COMPANY, INC.

Fig. 5-1. 10 - 15 μm glass spheres, 200 μm diameter orifice, 250 μm long

Fig. 5-2. 10 - 15 μm glass spheres, 343 μm diameter orifice, 125 μm long

5-3

Fig. 5-3. 10 - 15 μm glass spheres, 343 μm diameter orifice, 3.2 mm long

for the longer orifice with a second, somewhat broad peak appearing centered at 68 m/s. There is no escaping the conclusion, however, that particles are accelerated to a higher velocity with the longer orifice.

Figs. 5-4 and 5-5 show the effect of orifice length upon 13 μm polystryene spheres. Here again there is a peak velocity change from 85 m/s to 150 m/s. Note also that in this case there appears to be a peak at or near zero, which is discussed later. Figs. 5-6 and 5-7 show the orifice length effect for the 44 - 62 μm diameter glass spheres, showing once again an increase in peak velocity from 30 m/s to 45 m/s. Note also that the distributions do not drop off to zero quite as fast as for the smaller particles.

Figs. 5-8 and 5-9 show an increase in the high velocity tail effect. In fact, in Fig. 5-9, there is no well-defined velocity peak, only a long tail on the distribution. For the thinner leak shown in Fig. 5-8, a peak possibly exists at 40 m/s. However, it is clear that the velocity distribution tail extends further with the longer orifice. Note the different scale on the abscissa which goes to 400 m/s rather than 200 m/s as in all the other figures.

5.3   Particle Diameter

Next, the effect of particle diameter on velocity was investigated. Figs. 5-2, 5-6 and 5-8 show the velocity distributions for three different diameter glass spheres for the same 343 μm orifice in a 125 μm wall. In addition, we have Figs. 5-3, 5-7 and 5-9 for which the three particle sizes were used with the 343 μm orifice in the 3.2 mm wall. Here for both wall thicknesses the particle distribution changed from a peaked distribution for small particles to a long-tailed distribution for the larger particles. For small particles, the ratio of orifice to particle diameter is about 30:1, whereas, for the large particles it is 6:1 or 3:1.
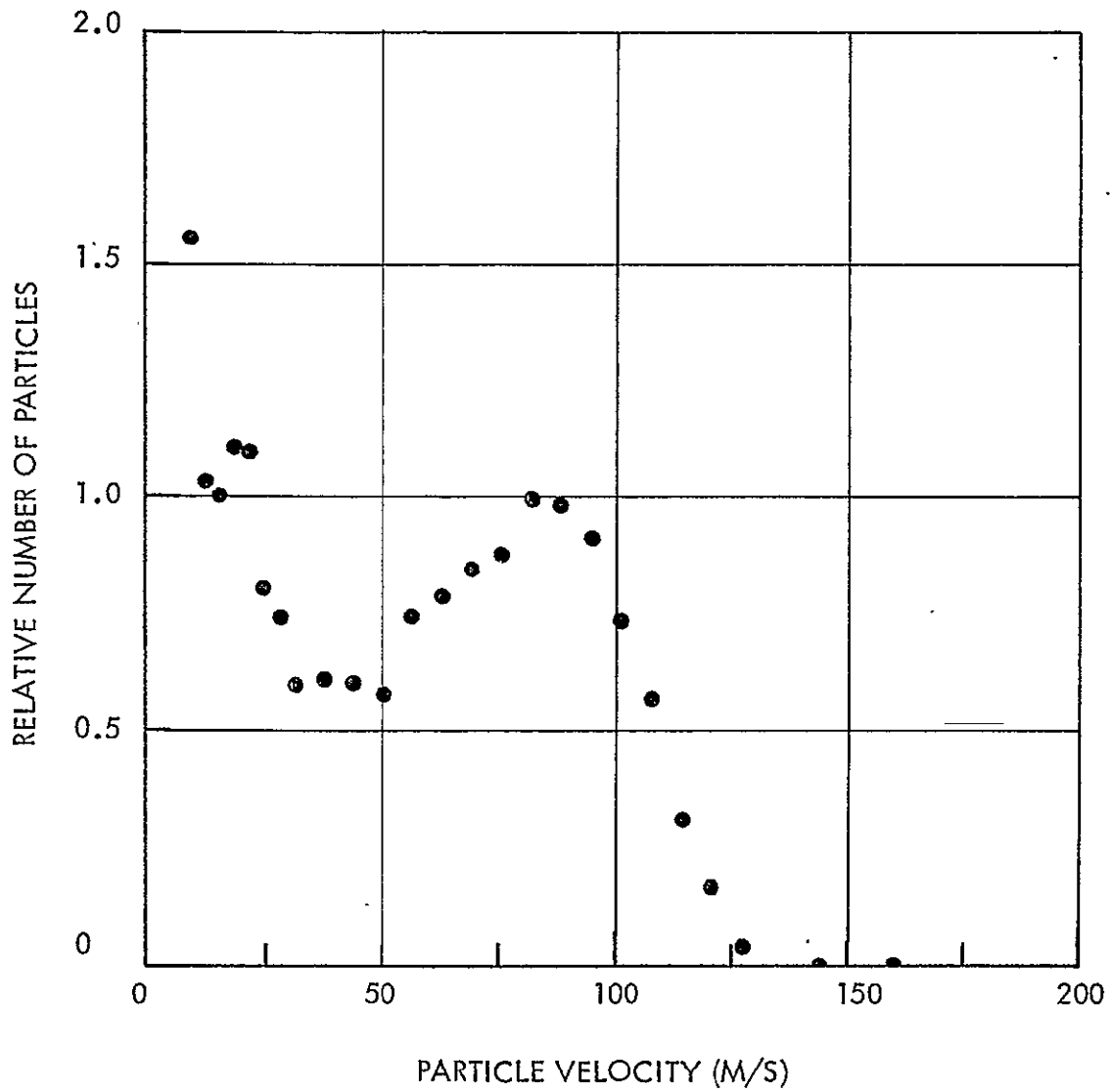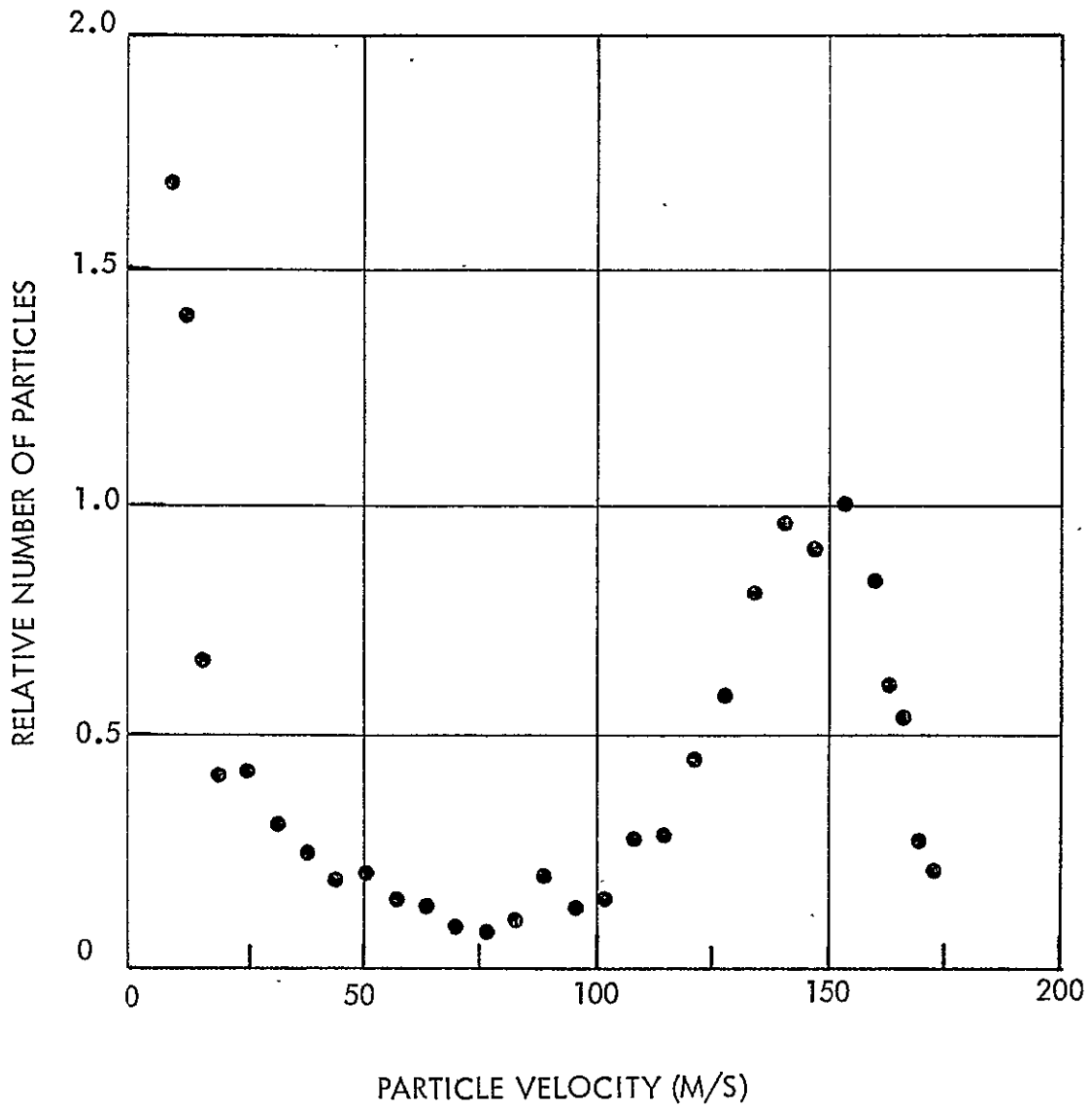
LOCKHEED MISSILES & SPACE COMPANY. INC.

Fig. 5-4. 13 μm polystyrene spheres, 343 μm diameter orifice, 125 μm long

LOCKHEED MISSILES & SPACE COMPANY, INC.

Fig. 5-5. 13 μm polystyrene spheres, 343 μm diameter orifice, 3.2 mm long
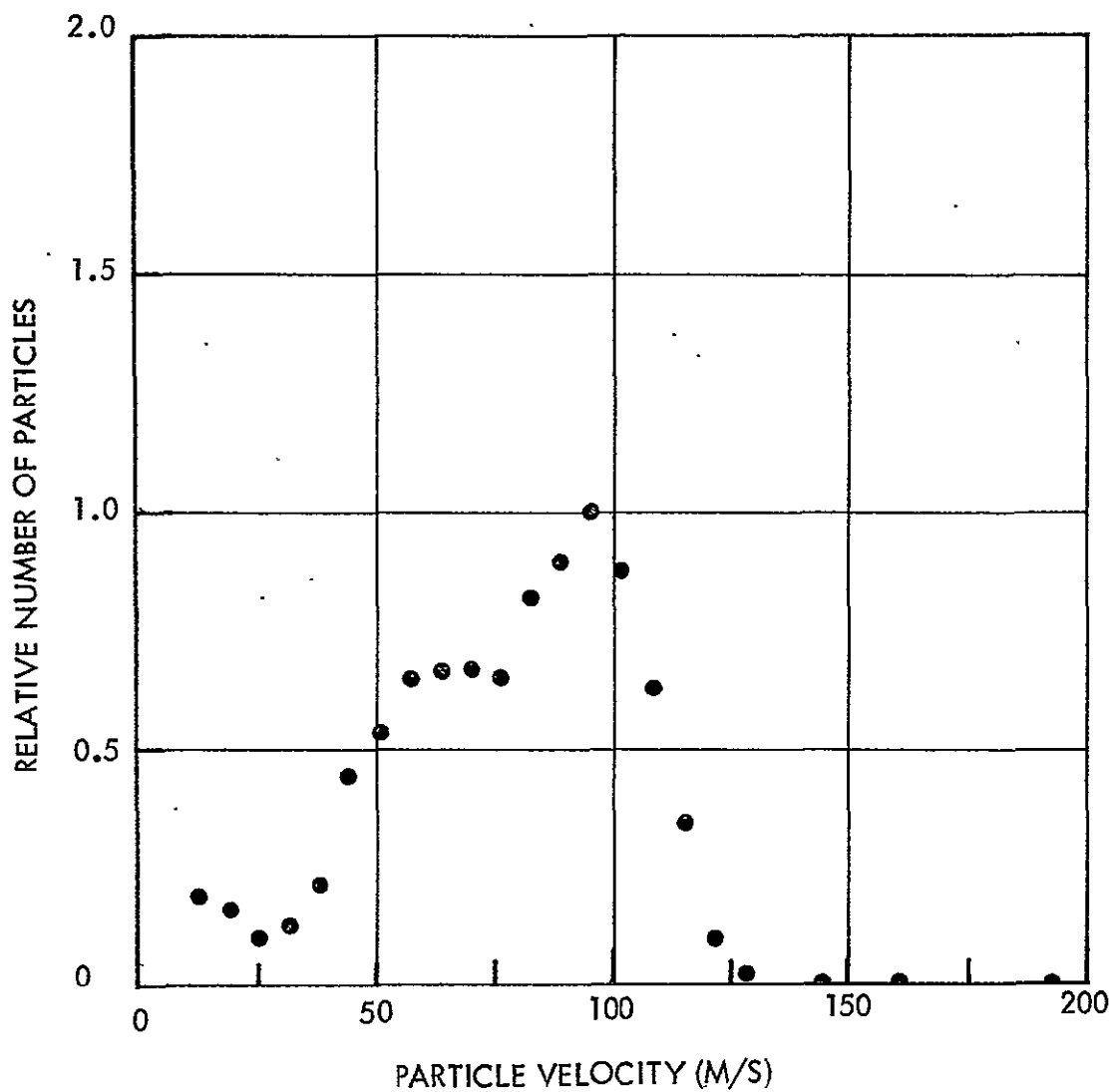
5-7

Fig. 5-6. 44 - 62 μm glass spheres, 343 μm diameter orifice, 125 μm long

5-8

Fig. 5-7. 44 - 62 μm glass spheres, 343 μm diameter orifice, 3.2 mm long
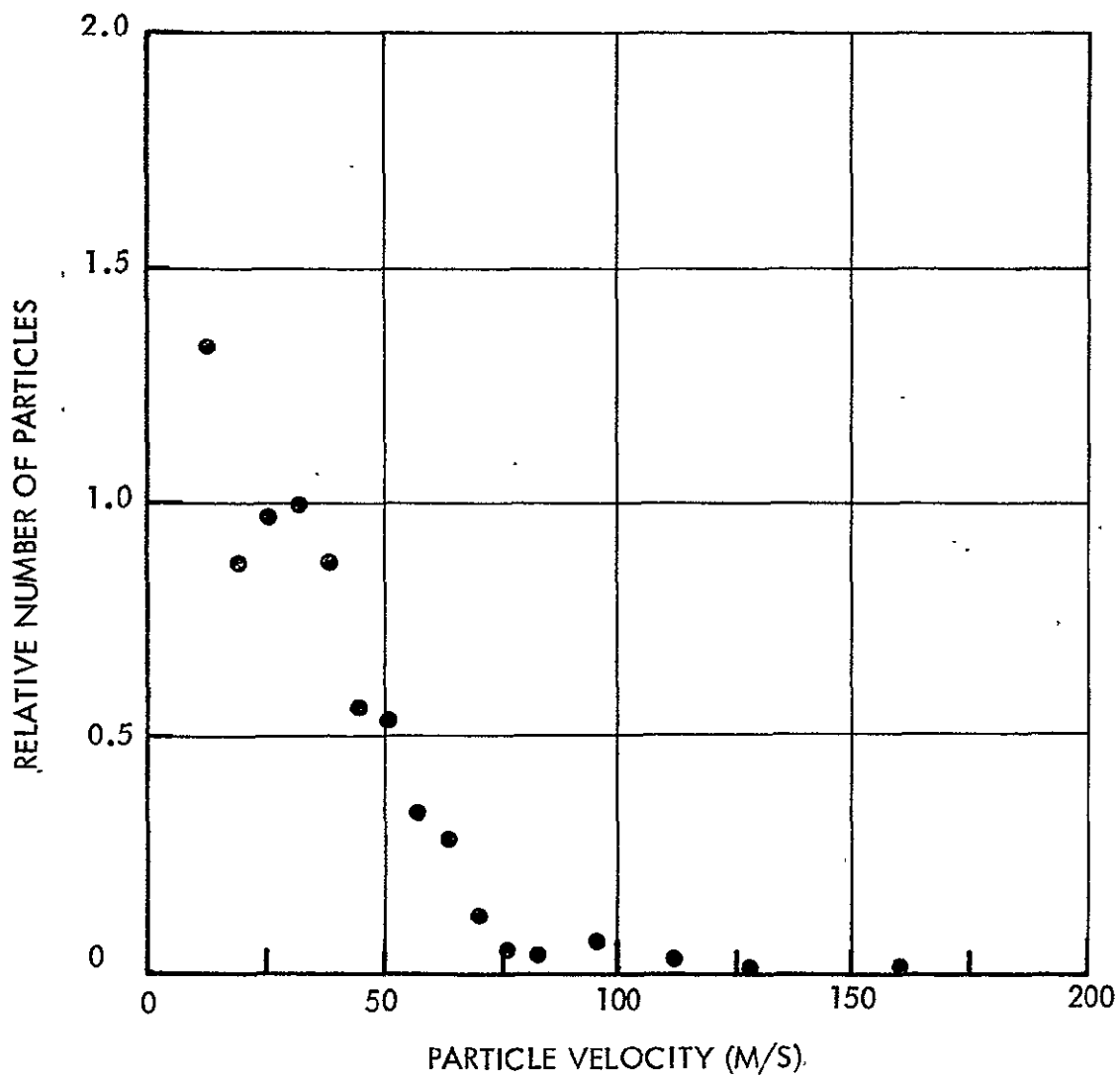
LOCKHEED MISSILES & SPACE COMPANY. INC.
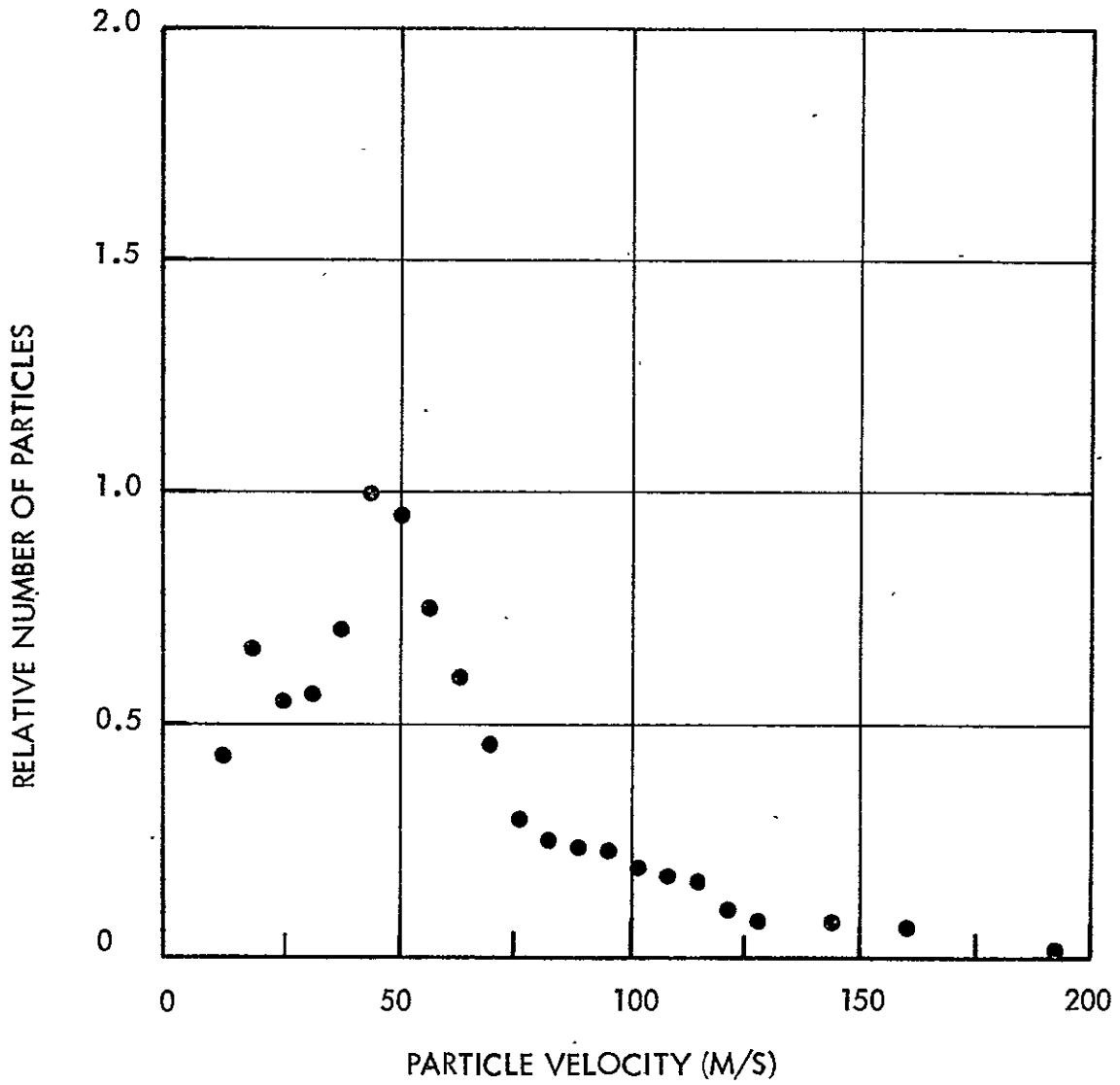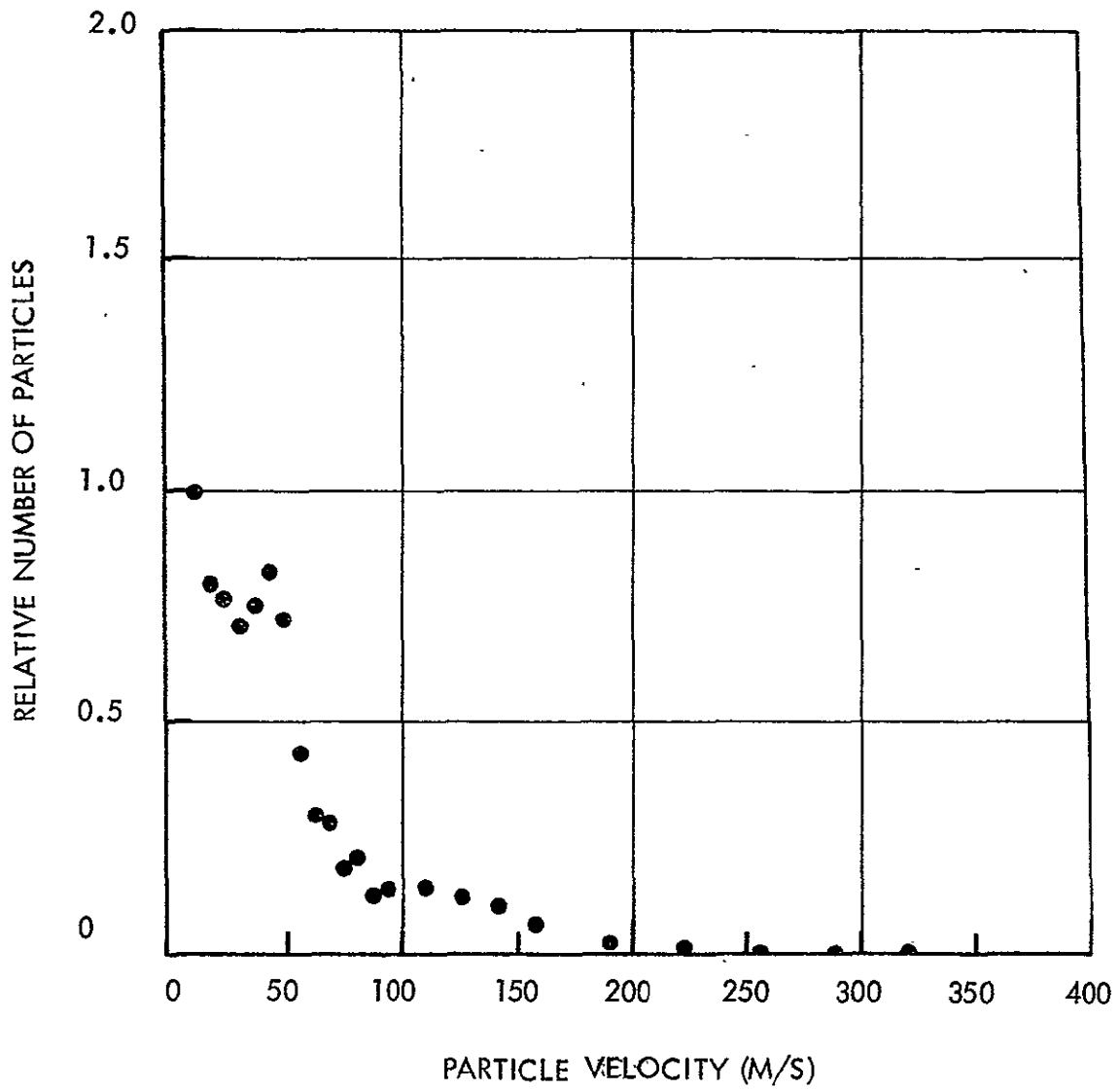
Fig. 5-8. 88 - 125 μm glass spheres, 343 μm diameter orifice, 125 μm long

Fig. 5-9. 88 - 125 μm glass spheres, 343 μm diameter orifice, 3.2 mm long

LOCKHEED MISSILES & SPACE COMPANY, INC.
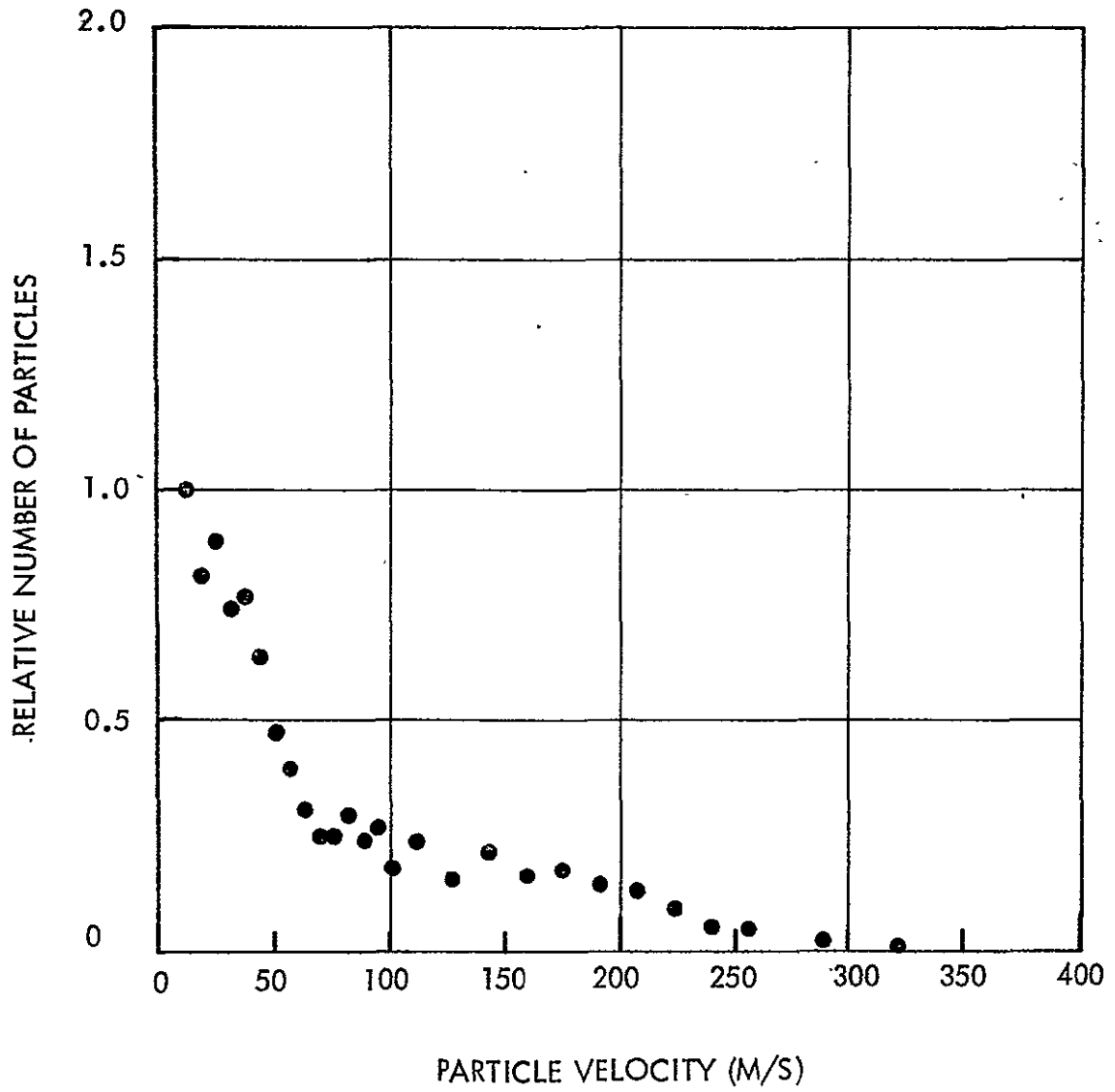
We believe the shape of the velocity distribution is directly attributable to this ratio, thus, if an orifice diameter of 3 mm were used, all particle diameters investigated would show a peaked distribution curve.

5.4   Particle Density

Finally, the effect of particle density on velocity distribution was investigated with 10 - 15 μm glass and 13 μm polystyrene spheres. The density of glass is about 2.5 gm/cm^3 while the density of polystyrene is about 0.9 gm/cm^3. Both particle species have diameters centered at 13 μm with the glass distributed over a range of 5 μm and the polystyrene distributed over about 2 - 3 μm. We believe that the effects noted below are due solely to density rather than diameter distribution. Figs. 5-2 and 5-4 for the 343 μm diameter orifice in the thin wall show a definite velocity increase from 40 m/s to 85 m/s. Figs. 5-3 and 5-5 show an increase in velocity from 96 m/s to 150 m/s. Note also the absence of the second broad peak in the lighter particle distribution. It is unclear why this broad peak is absent; however, there is no question that lower density particles are accelerated to greater velocities than are higher density particles.

Fig. 5-10 shows the particle distribution for the threaded NC 2-56 orifice with a bolt inserted 4 turns. Only with the 10 to 15 μm glass spheres were we able to obtain a sufficient number of particles to determine a distribution. The larger particles had insufficient room to pass through in large numbers and the polystyrene spheres seemed to adhere to the bolt and orifice surfaces and plugged the leak. Those particles which did pass through this leak did so at reduced velocities, peaking at about 20 m/s.

The last leak geometry investigated was the double wall simulated leak whose data are shown in Figs. 5-11 and 5-12 for a 343 μm diameter orifice in a 343 μm wall (on the high pressure side), followed by an offset 1 mm
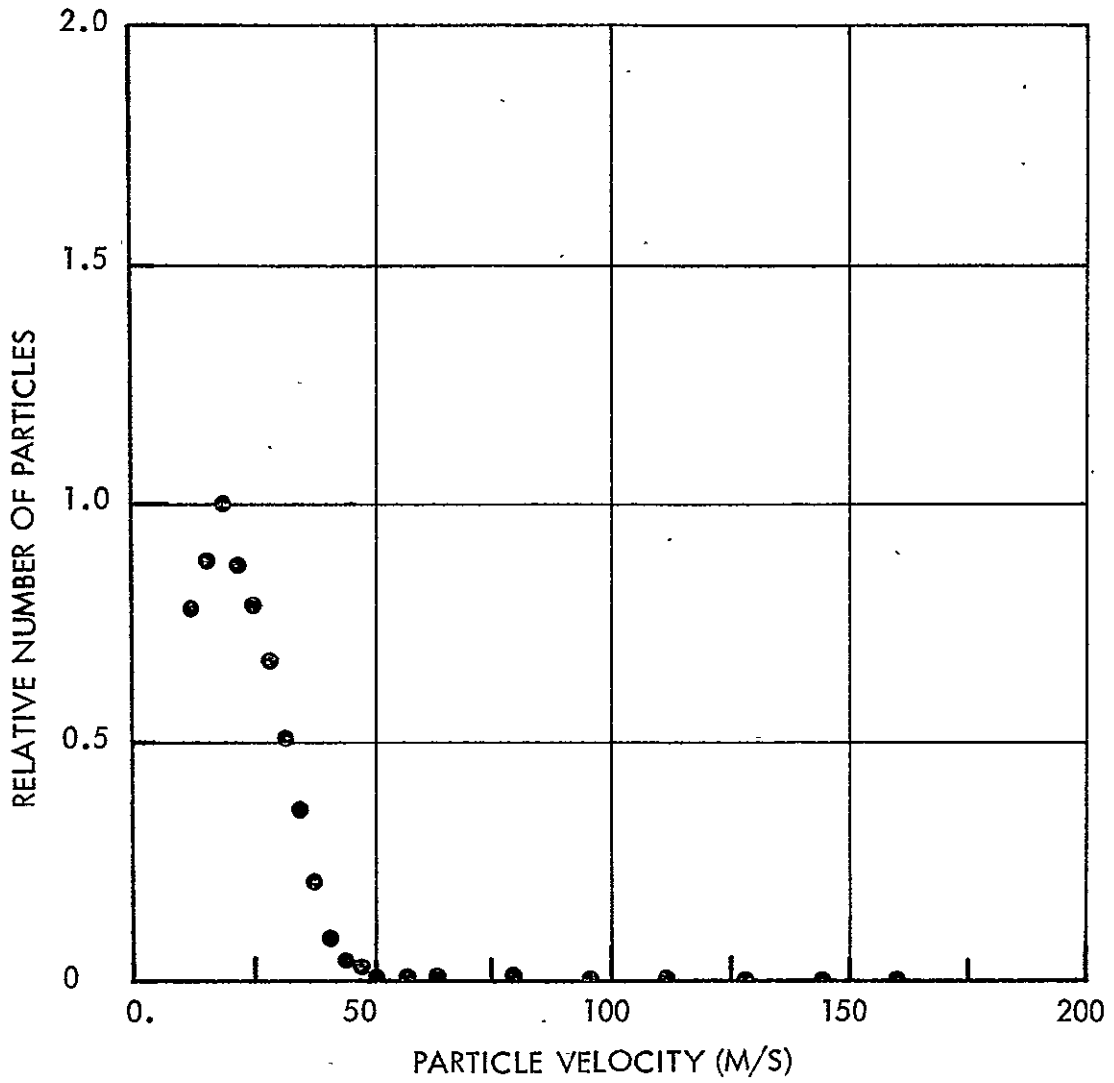
Fig. 5-10. 10 - 15 μm glass spheres, threaded orifice with bolt four turns in
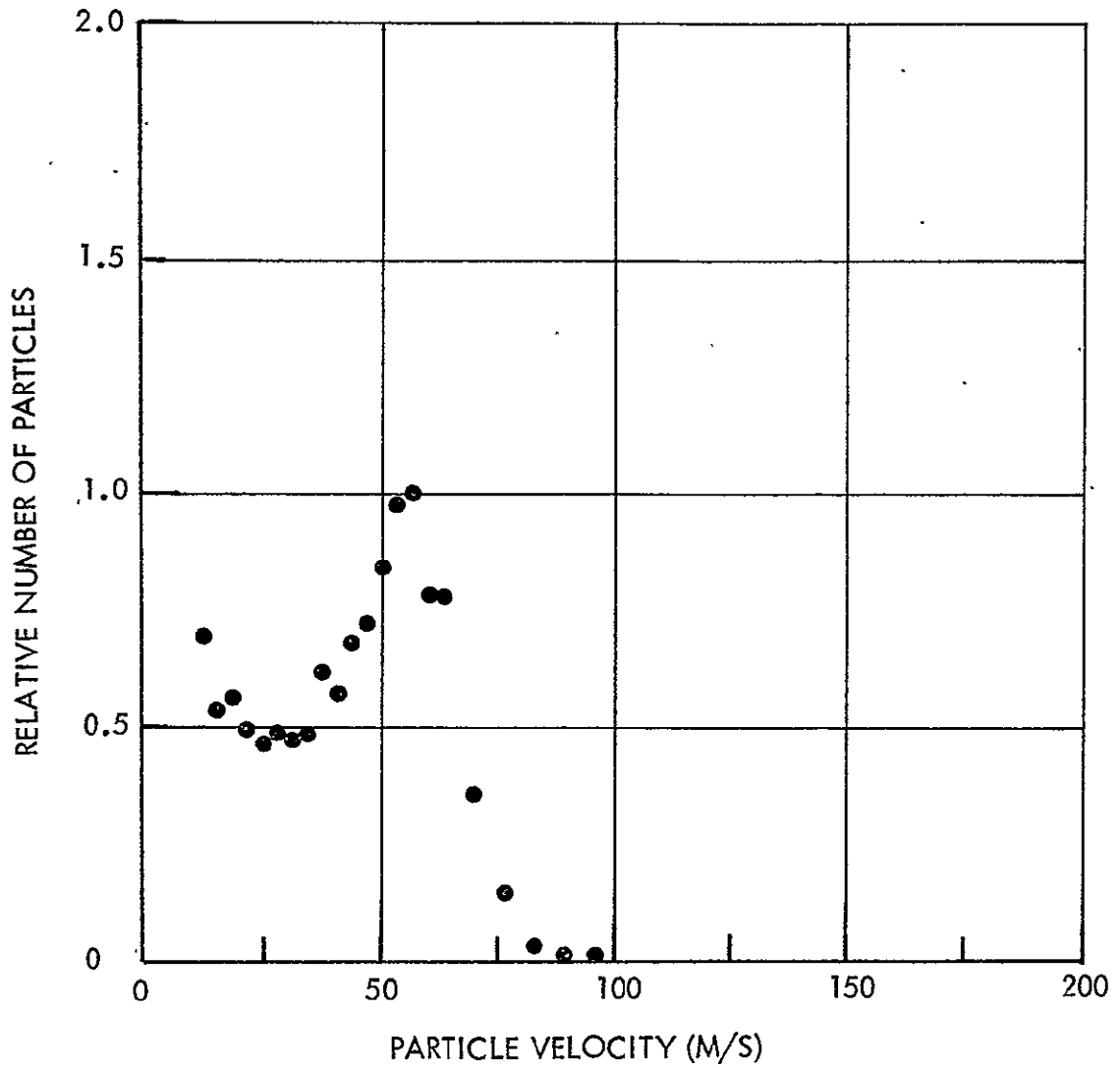
Fig. 5-11. 10 - 15 μm glass spheres, double walled leak, 343 μm & 1 mm
diameter orifices
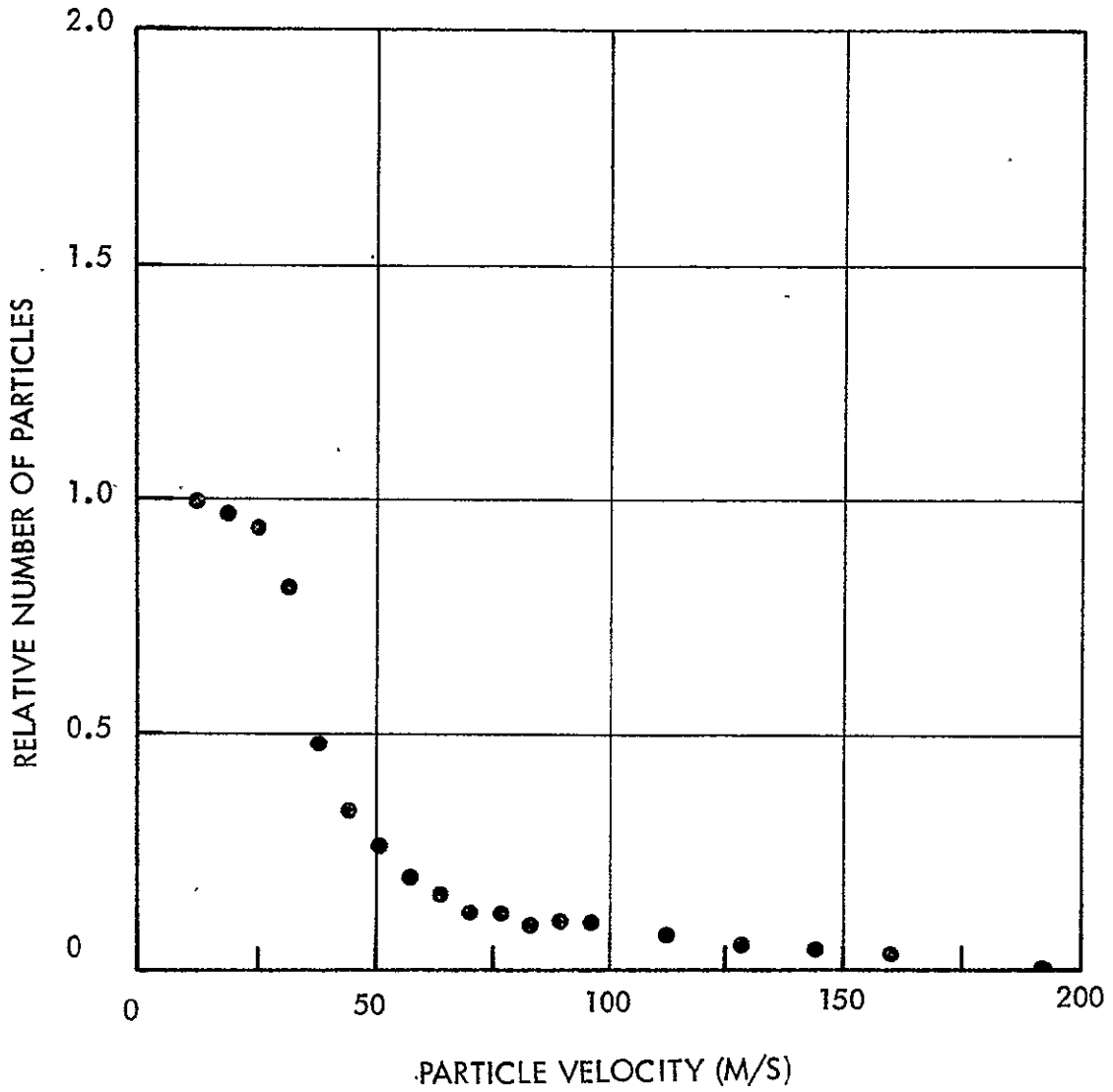
Fig. 5-12. 44 - 62 μm glass spheres, double walled leak, 343 μm & 1 mm
diameter orifices

5-15

LOCKHEED MISSILES & SPACE COMPANY. INC.

diameter orifice in a 3.5 mm wall. For the 10 - 15 μm glass spheres, the velocity distribution in Fig. 5-11 shows a peak near 58 m/s. The distribution in Fig. 5-12 for 44 - 62 μm glass spheres shows a possible peak near 15 m/s with the characteristic large particle velocity distribution tail.

After these data were taken, the second orifice was enlarged to 1.6 mm. Figs. 5-13 and 5-14 show velocity distributions for the 10-15 μm and 44-62 μm diameter glass spheres respectively. For the smaller particles, there is a definite reduction in the peak velocity from 58 m/s to 33 m/s. For the large particles, the change is almost undetectable, except for only one change in the lowest velocity data point. The velocity distribution for the larger particles shows the characteristic tail at high velocities.

Data taken early in the study always showed a large number of particles at velocities below 15 m/s independent of leak geometry or particle species. It developed that these numbers could be reduced by preventing particles from bouncing off the chamber walls and reentering the scattering region at reduced velocity and/or at angles other than the expected ones. Coating the walls with felt accomplished this. It is possible however, that some particles which appear in the velocity distributions shown here have suffered at least one wall collision before entering the scattering region. As a consequence, the data below 15 m/s is felt to be of doubtful validity.

It is important to note that the absence of data points at high velocities does not indicate that no particles were observed at that velocity. Although a small fraction always appeared at high velocities for most leak geometries and particle species, the data were not taken because an insufficient number of particles per burst were obtained to provide a valid distribution.
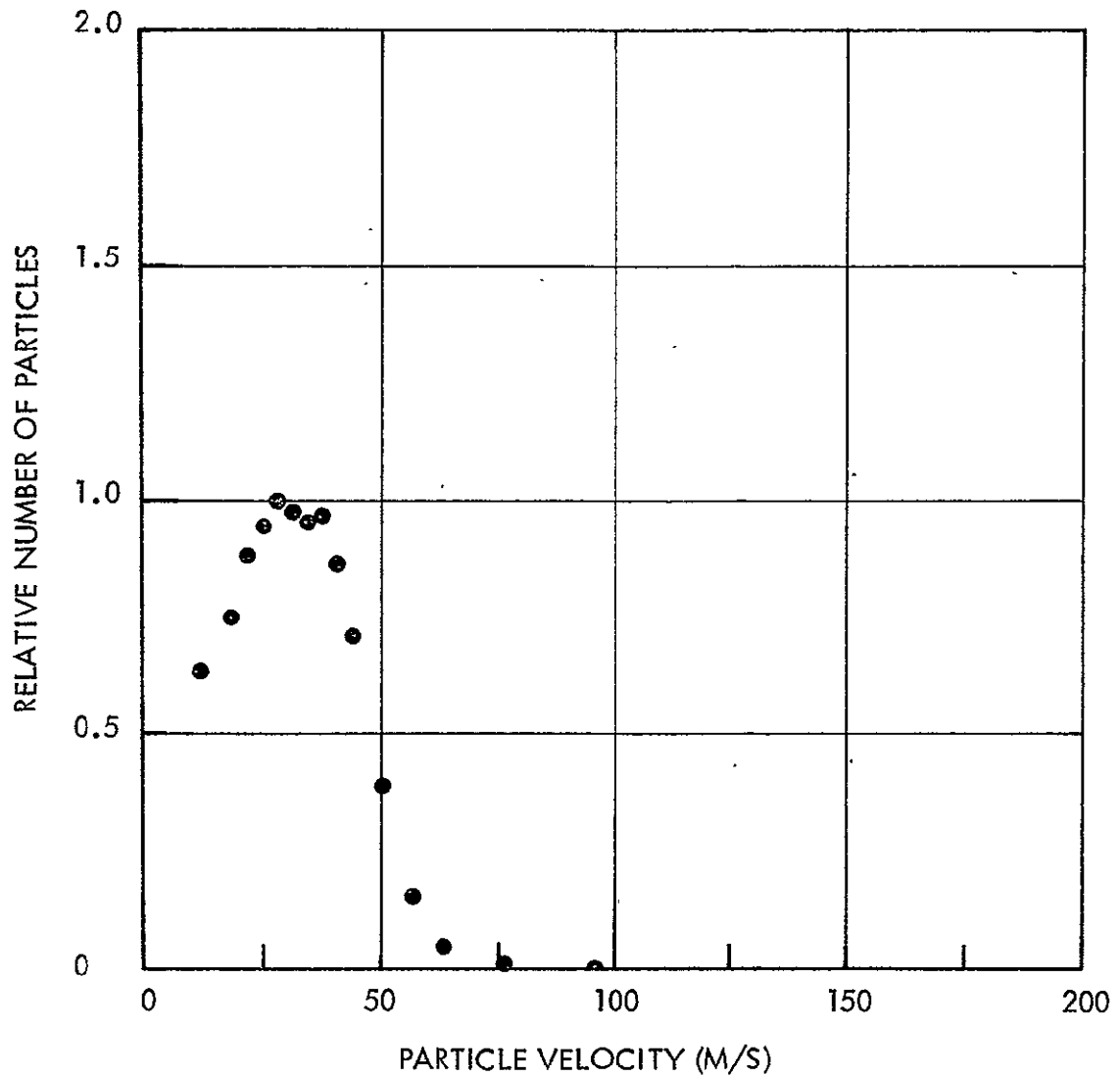
Fig. 5-13. 10 - 15 μm glass spheres, double walled leak, 343 μm & 1.6 mm diameter orifices
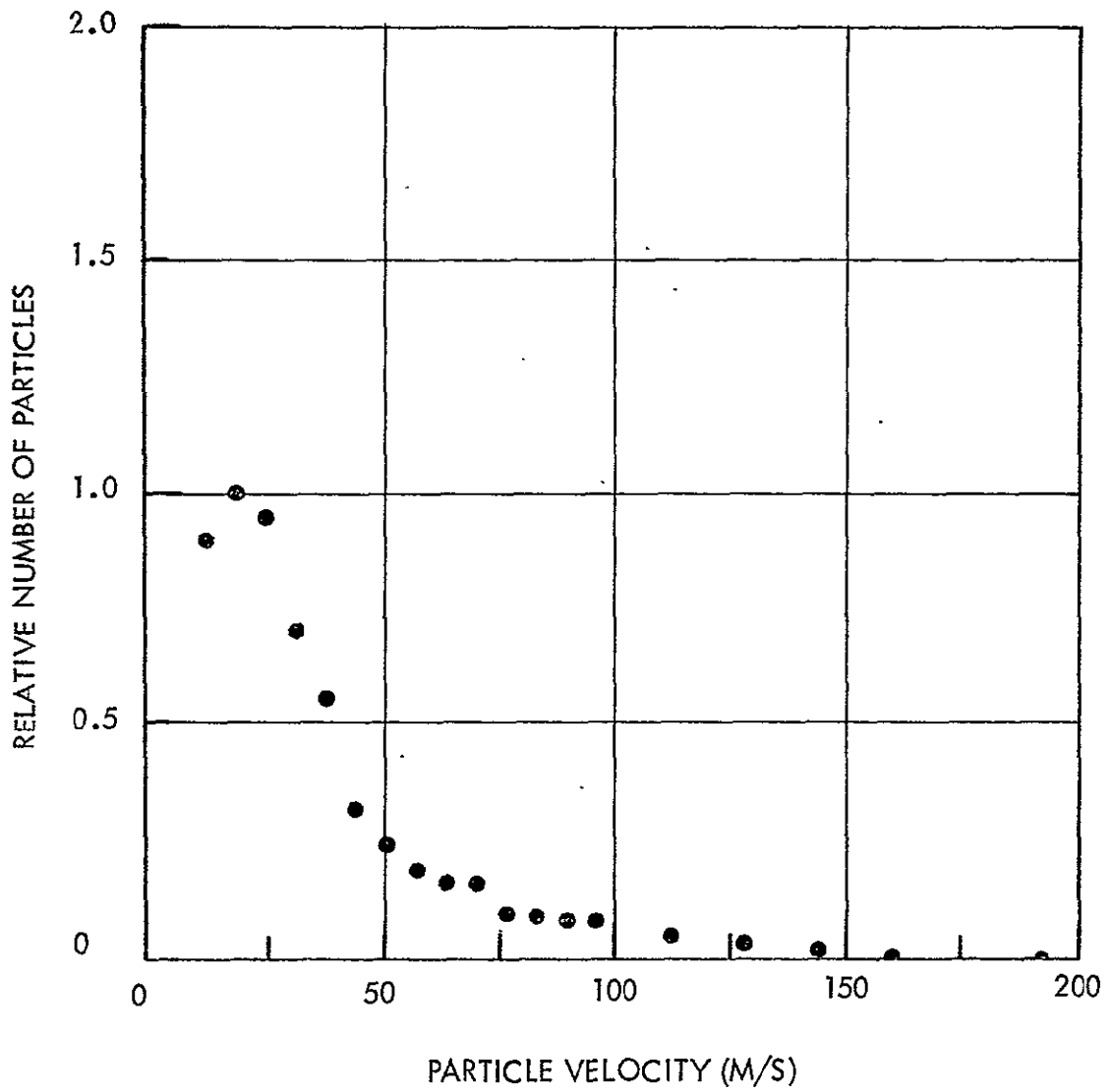
5-17

LOCKHEED MISSILES & SPACE COMPANY, INC.

Fig. 5-14. 44 - 62 μm glass spheres, double walled leak, 343 μm & 1.6 mm diameter orifices

LOCKHEED MISSILES & SPACE COMPANY, INC.

Section 6

CONCLUSIONS AND RECOMMENDATIONS

This report describes the use of a Laser Doppler Velocimeter to measure the velocity distributions of particles leaking into a vacuum chamber to simulate dust contaminants escaping from the Space Shuttle into space. Velocity distributions for four particle species and six leak geometries are reported. Glass spheres with the diameters of 13, 53, and 106 μm diameters and polystyrene spheres with a 13 μm diameter were used. A velocity range from 15 to 320 m/s was investigated.

It was found that the distributions for smaller particles peaked at velocities in the 15 to 150 m/s range. Larger particle distributions tended to spread over a wider velocity range with numbers of particles decreasing as velocities increased. In the 150 to 320 m/s range, the 106 μm diameter glass spheres had significant numbers while the 13 μm spheres had very few.

Particle velocity is independent of orifice diameter for leaks in thin walls provided the orifice is much larger than the particle diameter. Leaks through thick walls accelerate particles to higher velocities than do leaks through thin walls. Finally, lower density particles are accelerated to higher velocities than are higher density particles.

Experience indicates a few ways in which these experimental investigations can be extended or improved. We measured only the velocities of particles which exited a leak in a direction normal to the wall. We believe a measurement of the angular distribution of directions for the escaping particles would provide interesting and useful data to help explain, for example, the effect double walls have on shielding or preventing high velocity particles from escaping.

LOCKHEED MISSILES & SPACE COMPANY, INC.

In the work completed, the largest particle diameters were about 1/3 the diameter of the leak orifice in some cases, while the smallest particles were 1/300 the orifice diameter. We believe the velocity distribution curves change from a peaked distribution for small diameters to a mono-tonically decreasing distribution for large diameters. The use of one or more small diameter particle sizes could verify this assumption.

The signal processor used in this work utilized two channels, one of which counted particles in a fixed velocity interval and the other which counted particles in a velocity interval which could be varied over the entire range of interest. The first channel was used to give an indication of the total number of particles dispensed and the second, in conjunction with the first, gave the particle velocity distribution.

Data accummulation could be facilitated enormously by utilizing many more channels so that the entire velocity range of interest could be covered continuously. The time required to produce one particle velocity distribution with an N channel processor would be reduced 1/N times the time required to take N data points with a two channel processor.

APPENDIX

The raw experimental data used to produce the results presented in
Section 5 are tabulated in this Appendix. The center frequency of the
tunable filter in the variable channel is listed in the first column.
The number of particle count per particle surge is listed next for the
variable channel and fixed channel respectively. The final column lists
the sum total of the variable channel count divided by the sum total of
the fixed channel count.

LOCKHEED MISSILES & SPACE COMPANY. INC.

Table A-1: Data for Fig. 5-1

Freq. MHz	No. of Particles in Variable Channel (V)	No. of Particles in Fixed Channel (F)	Ratio V/F
0.4	50, 106	511, 742	.125
0.5	73, 130	793, 781	.129
0.6	74, 332	473, 851	.307
0.7	177, 366	657, 856	.359
0.8	284, 502	688, 846	.512
0.9	313, 550	555, 827	.624
1.0	390, 597	657, 836	.661
1.1	277, 493	488, 742	.626
1.2	406, 552	667, 824	.643
1.3	355, 589	590, 895	.636
1.4	214, 598	366, 815	.688
1.5	266, 504	450, 779	.627
1.6	369, 557	656, 822	.627
1.7	232, 464	586, 832	.491
1.8	208, 291	759, 814	.317
1.9	83, 96	706, 608	.136
2.0	49, 14	852, 291	.055
2.25	6, 5	652, 304	.012
2.50	3, 6	467, 430	.010
2.75	6, 7	581, 441	.013
3.0	4, 6	609, 453	.009
3.5	5, 6	652, 559	.009
4.0	4, 10	495, 670	.012
4.5	4, 8	423, 617	.011
5.0	3, 1	423, 596	.004
6.0	0	520	.000
7.0	0	482	.000
8.0	0	441	.000
9.0	0	613	.000
10.0	0	545	.000

A-2

LOCKHEED MISSILES & SPACE COMPANY. INC.

Table A-2:   Data for Fig. 5-2

Freq. MHz	No. of Particles in Variable Channel (V)	No. of Particles in Fixed Channel (F)	Ratio V/F
0.4	366, 157, 308	1152, 843, 1110	.268
0.6	292, 89, 174	1196, 718, 942	.194
0.8	405, 427, 394	1040, 1021, 957	.406
1.0	593, 434, 582	966, 801, 1031	.575
1.2	836, 617, 563, 594	1204, 925, 925, 883	.663
1.4	657, 1001, 881	1021, 1614, 1258	.652
1.6	729, 703, 655	1070, 1200, 1060	.626
1.8	438, 362, 445	950, 935, 1011	.430
2.0	259, 193, 209	1055, 1141, 1158	.197
2.2	47, 25, 27	925, 743, 864	.039
2.4	10	914	.011
2.6	4	692	.006
3.0	8	664	.012
4.0	7	818	.009
5.0	0	833	.000

Table A-3: Data for Fig. 5-3

Freq. MHz	No. of Particles in Variable Channel (V)	No. of Particles in Fixed Channel (F)	Ratio V/F
0.4	172, 315, 104	1785, 1887, 1104	.124
0.6	261, 166	2191, 1914	.104
0.8	189, 59	1933, 1691	.068
1.0	202, 132	2048, 1905	.084
1.2	271, 217	1782, 1732	.139
1.4	603, 492	1942, 1883	.286
1.6	652, 679	1943, 1930	.344
1.8	736, 794	1836, 1824	.418
2.0	909, 740	2118, 1734	.428
2.2	831, 748	2005, 1651	.432
2.4	830, 798	1950, 1928	.420
2.6	917, 963	1726, 1826	.529
2.8	1140, 1053	1893, 1917	.576
3.0	1362, 1021	2053, 1636	.646
3.2	1000, 893	1766, 1590	.564
3.4	694, 587	1710, 1462	.404
3.6	447, 268	1781, 1437	.222
3.8	139, 65	1847, 1268	.065
4.0	45, 18	2037, 1496	.018
4.5	10	1794	.006
5.0	14	1765	.008
6.0	7	1449	.005
7.0	5	1626	.003
8.0	0	1916	.000
9.0	0	1683	.000

Table A-4: Data for Fig. 5-4

Freq. MHz	No. of Particles in Variable Channel (V)	No. of Particles in Fixed Channel (F)	Ratio V/F
0.3	3474	3745	.928
0.4	2279	3688	.618
0.5	1835	3056	.600
0.6	1894	2860	.662
0.7	1888	2883	.655
0.8	1237	2574	.481
0.9	1110	2511	.442
1.0	742	2074	.358
1.2	849	2328	.365
1.4	682	1894	.360
1.6	631	1829	.345
1.8	763	1710	.446
2.0	797	1690	.472
2.2	713	1420	.502
2.4	1609	3051	.527
2.6	1658	2791	.594
2.8	1529	2607	.586
3.0	1306	2399	.544
3.2	943	2148	.439
3.4	630	1853	.340
3.6	313	1681	.186
3.8	151	1465	.103
4.0	30	1096	.027
4.5	0	882	.000
5.0	1	1385	.0007

A-5

Table A-5: Data for Fig. 5-5

Freq. MHz	No. of Particles in Variable Channel (V)	No. of Particles in Fixed Channel (F)	Ratio V/F
0.3	1677	747	2.245
0.4	1601	860	1.862
0.5	1115	1273	.876
0.6	438	797	.550
0.8	519	917	.566
1.0	270	656	.412
1.2	145	439	.330
1.4	116	454	.256
1.6	196	711	.276
1.8	138	687	.201
2.0	163	897	.182
2.2	120	958	.125
2.4	23, 108	259, 942	.109
2.6	77	531	.145
2.8	146	545	.268
3.0	53	295	.180
3.2	90	429	.210
3.4	200	537	.372
3.6	172	445	.387
3.8	254	422	.602
4.0	278	354	.785
4.2	485	449	1.080
4.4	593	463	1.281
4.6	616	513	1.201
4.8	620	465	1.333
5.0	919	829	1.109
5.1	248	306	.810
5.2	528	733	.720
5.3	78	202	.368
5.4	219	765	.286

A-6

Table A-6: Data for Fig. 5-6

Freq. MHz	No. of Particles in Variable Channel (V)	No. of Particles in Fixed Channel (F)	Ratio V/F
0.4	95, 41, 24, 75, 70, 80	119, 47, 79, 187, 170, 229	.463
0.6	25, 18, 42, 50, 58, 67	88, 102, 129, 141, 206, 193	.303
0.8	53, 25, 38, 75, 37, 51	145, 89, 120, 179, 125, 168	.338
1.0	14, 38, 40, 81, 71, 38	62, 88, 113, 236, 187, 126	.347
1.2	47, 34, 54, 53, 27	136, 133, 159, 177, 103	.304
1.4	29, 29, 39, 24, 17	97, 145, 199, 145, 113	.197
1.6	60, 47, 19, 15, 21	256, 212, 68, 129, 195	.188
1.8	20, 28, 26, 23, 23	142, 213, 251, 207, 192	.119
2.0	63, 18, 17, 15, 11	416, 176, 262, 221, 170	.100
2.2	5, 13, 8, 4, 7	123, 205, 133, 205, 167	.044
2.4	9, 3, 3, 0	226, 175, 165, 191	.020
2.6	5, 1, 1, 2	176, 169, 140, 107	.015
3.0	4, 2, 3, 1	130, 122, 87, 64	.025
3.5	1, 2	148, 102	.012
4.0	3, 0	324, 196	.006
5.0	2, 1	188, 271	.007

Table A-7: Data for Fig. 5-7

Freq. MHz	No. of Particles in Variable Channel (V)	No. of Particles in Fixed Channel (F)	Ratio V/F
0.4	122, 188, 105, 380, 126	286, 386, 192, 875, 391	.432
0.6	49, 31, 27, 301, 85	194, 102, 136, 776, 304	.326
0.8	12, 31, 27, 235, 49	62, 141, 228, 645, 228	.271
1.0	6, 80, 53, 131, 216, 78	59, 384, 277, 547, 506, 245	.279
1.2	74, 205, 66, 246, 109	300, 544, 289, 515, 353	.349
1.4	95, 269, 307, 288, 81	282, 531, 559, 541, 201	.492
1.6	108, 281, 278, 244, 104	249, 564, 560, 524, 269	.469
1.8	136, 217, 210, 176, 54	321, 585, 542, 517, 184	.369
2.0	120, 170, 170, 133	379, 533, 571, 530	.295
2.2	29, 105, 141, 134	114, 532, 587, 582	.225
2.4	24, 84, 96, 67	208, 549, 576, 512	.147
2.6	36, 77, 69, 72	403, 537, 537, 576	.124
2.8	30, 86, 58, 42	316, 525, 511, 517	.116
3.0	18, 92, 54, 39	244, 535, 491, 519	.113
3.2	11, 45, 52	181, 461, 499	.095
3.4	25, 35, 40	259, 480, 412	.087
3.6	2, 77, 41, 28	87, 523, 659, 604	.079
3.8	3, 27, 34	114, 584, 555	.051
4.0	8, 20, 22	230, 520, 500	.040
4.5	18, 21	497, 498	.039
5.0	22, 11	487, 512	.033
6.0	2, 8	475, 511	.010
7.0	8, 5	574, 517	.012
8.0	2, 3	482, 512	.005
9.0	0, 1	442, 461	.001
10.0	0, 0	469, 497	.000

Table A-8: Data for Fig. 5-8

Freq. MHz	No. of Particles in Variable Channel (V)	No. of Particles in Fixed Channel (F)	Ratio V/F
0.4	100, 103, 86, 90, 83	241, 307, 321, 312, 239	.325
0.6	70, 64, 68, 56, 64	253, 266, 303, 219, 199	.260
0.8	68, 69, 46, 57, 60	226, 264, 240, 227, 242	.250
1.0	74, 74, 62, 43, 29	286, 324, 241, 201, 176	.230
1.2	88, 69, 70, 26, 32	353, 301, 272, 117, 120	.245
1.4	56, 60, 32, 33, 62	244, 228, 154, 123, 156	.269
1.6	41, 92, 64, 51, 28	221, 402, 292, 138, 117	.236
1.8	30, 37, 39, 23, 23	249, 208, 248, 107, 223	.141
2.0	37, 23, 19, 20, 9	268, 224, 237, 192, 180	.098
2.2	21, 18, 27, 39, 18	250, 240, 279, 348, 224	.092
2.4	24, 18, 7, 10, 11	284, 236, 219, 205, 198	.061
2.6	22, 11, 15, 11, 18	241, 222, 276, 175, 193	.070
2.8	9, 10, 11, 11, 8	246, 287, 239, 210, 187	.042
3.0	20, 10, 7, 7, 7	233, 254, 199, 189, 221	.047
3.5	17, 12, 16, 15, 5	323, 241, 329, 285, 215	.047
4.0	10, 21, 13, 3, 9	251, 531, 240, 188, 167	.041
4.5	6, 13, 10, 9, 9	201, 224, 343, 431, 149	.035
5.0	6, 6, 3, 4, 5	213, 299, 244, 169, 179	.022
6.0	3, 3, 1	254, 272, 158	.010
7.0	3, 1, 0	252, 266, 160	.006
8.0	0, 0	243, 260	.000
9.0	1, 0	360, 218	.002
10.0	0, 0	319, 221	.000

Table A-9: Data for Fig. 5-9

Freq. MHz	No. of Particles in Variable Channel (V)	No. of Particles in Fixed Channel (F)	Ratio V/F
0.4	86, 59, 85, 75, 59, 84	129, 94, 131, 104, 81, 137	.663
0.6	55, 58, 133, 51, 57, 48	104, 94, 284, 87, 88, 89	.539
0.8	51, 93, 81, 65, 53, 49	88, 183, 162, 86, 65, 80	.590
1.0	37, 68, 52, 190, 67, 51	108, 137, 112, 346, 142, 100	.492
1.2	43, 62, 57, 51, 73, 40	79, 132, 113, 102, 122, 90	.511
1.4	35, 39, 28, 35, 48, 43	86, 104, 85, 82, 100, 83	.422
1.6	25, 34, 29, 29, 25, 25	80, 98, 96, 75, 95, 89	.313
1.8	28, 21, 26, 25, 28, 16	87, 86, 99, 91, 101, 81	.264
2.0	15, 14, 22, 21, 8, 15	83, 69, 102, 71, 65, 71	.206
2.2	15, 21, 16, 17, 15, 13	98, 119, 99, 100, 80, 91	.165
2.4	13, 18, 18, 18, 15, 12	76, 117, 88, 86, 105, 89	.168
2.6	21, 27, 29, 13, 9, 11	101, 96, 137, 82, 75, 61	.199
2.8	16, 21, 27, 14, 12, 6	104, 124, 135, 94, 76, 72	.159
3.0	22, 32, 26, 14, 17, 9	109, 133, 157, 68, 115, 86	.180
3.2	11, 18, 13, 19, 16, 4	127, 125, 106, 118, 110, 78	.122
3.5	16, 17, 13, 40, 26, 4	117, 116, 91, 162, 157, 90	.158
4.0	24, 12, 8, 14, 8, 6	116, 94, 95, 169, 108, 84	.108
4.5	15, 35, 34, 17, 17, 5	103, 293, 193, 106, 80, 77	.144
5.0	8, 16, 11, 9, 10, 8	102, 103, 109, 85, 104, 66	.109
5.5	12, 7, 21, 11, 8	93, 109, 89, 98, 108	.119
6.0	19, 7, 9, 6, 3	132, 76, 77, 95, 75	.097
6.5	7, 9, 8	106, 90, 83	.086
7.0	8, 7, 8	178, 97, 92	.063
7.5	1, 7, 3	150, 93, 75	.035
8.0	5, 3, 2	131, 70, 81	.035
9.0	2, 3, 0	124, 71, 100	.017
10.0	0, 0, 2	97, 71, 67	.009

Table A-10: Data for Fig. 5-10

Freq. MHz	No. of Particles in Variable Channel (V)	No. of Particles in Fixed Channel (F)	Ratio V/F
0.4	70, 272	112, 275	.884
0.5	143, 328	214, 256	1.002
0.6	262, 224, 184	270, 176, 145	1.134
0.7	237, 235, 219	290, 203, 205	.990
0.8	298, 172, 194	332, 188, 222	.895
0.9	216, 103, 108	286, 136, 138	.763
1.0	210, 117, 40	336, 185, 113	.579
1.1	181, 45, 72	371, 161, 197	.409
1.2	106, 32, 24	335, 189, 151	.240
1.3	37, 22, 16	293, 202, 186	.110
1.4	16, 14, 6	294, 183, 176	.055
1.5	14, 6	315, 187	.040
1.6	5, 2	278, 150	.016
1.8	5, 2	251, 168	.017
2.0	3, 5	278, 175	.018
2.5	5, 3	312, 140	.018
3.0	3, 1	296, 159	.009
3.5	3, 0	284, 165	.007
4.0	1, 0	257, 157	.002
4.5	0, 1	181, 149	.003
5.0	0, 0	250, 125	.000

Table A-11: Data for Fig. 5-11

Freq. MHz	No. of Particles in Variable Channel (V)	No. of Particles in Fixed Channel (F)	Ratio V/F
0.4	346, 764	1116, 2186	.336
0.5	258, 546	1029, 2060	.260
0.6	311, 453	1050, 1755	.272
0.7	241, 436	1080, 1755	.239
0.8	175, 468	921, 1949	.224
0.9	207, 475	1022, 1861	.237
1.0	126, 487	867, 1817	.228
1.1	252, 368	1220, 1421	.235
1.2	405, 524	1419, 1684	.299
1.3	330	1193	.277
1.4	355, 561	1182, 1597	.330
1.5	366	1047	.350
1.6	429, 727	1180, 1663	.407
1.7	386, 775	893, 1580	.469
1.8	362, 878	864, 1704	.483
1.9	327	866	.378
2.0	246, 577	821, 1370	.376
2.2	127, 293	833, 1603	.172
2.4	48, 121	814, 1555	.071
2.6	7, 38	790, 1656	.018
2.8	4, 16	779, 1360	.009
3.0	3, 12	710, 1216	.008

Table A-12: Data for Fig. 5-12

Freq. MHz	No. of Particles in Variable Channel (V)	No. of Particles in Fixed Channel (F)	Ratio V/F
0.4	308, 454	496, 528	.744
0.6	342, 512	580, 601	.723
0.8	398, 418	620, 544	.701
1.0	323, 335	552, 533	.606
1.2	211, 188	550, 558	.360
1.4	157, 138	604, 562	.353
1.6	107, 95	518, 506	.197
1.8	86, 82	515, 598	.151
2.0	64, 76	561, 578	.123
2.2	53, 52	586, 537	.074
2.4	61, 49	610, 559	.094
2.6	41, 36	532, 521	.073
2.8	55, 38	599, 543	.081
3.0	39, 50	575, 574	.074
3.5	33, 31	558, 533	.059
4.0	23, 22	516, 537	.043
4.5	16, 23	572, 554	.035
5.0	18, 12	541, 508	.029
6.0	3, 3	527, 534	.006

Table A-13: Data for Fig. 5-13

Freq. MHz	No. of Particles in Variable Channel (V)	No. of Particles in Fixed Channel (F)	Ratio V/F
0.4	838, 776	1854, 1835.	.438
0.6	1013, 982	1869, 1993	.517
0.7	1058, 1118	1773, 1800	.609
0.8	1365, 1182	2136, 1757	.654
0.9	1083, 1176	1613, 1658	.691
1.0	1313, 1156	1980, 1689	.673
1.1	1013, 1241	1624, 1802	.658
1.2	1221, 991	1863, 1489	.660
1.3	1143, 973	1959, 1598	.595
1.4	1028, 705	1946, 1604	.488
1.6	624, 277	1916, 1450	.268
1.8	279, 104	2037, 1597	.105
2.0	79, 29	1886, 1522	.032
2.4	14, 12	1857, 1402	.008
3.0	10, 5	1915, 1536	.004

Table A-14:   Data for Fig. 5-14

Freq. MHz	No. of Particles in Variable Channel (V)	No. of Particles in Fixed Channel (F)	Ratio V/F
0.4	280, 311, 516, 603	305, 352, 1139, 678	.691
0.6	310, 539, 535	321, 819, 660	.769
0.8	256, 424, 489	346, 620, 639	.728
1.0	135, 370, 381	287, 682, 666	.542
1.2	116, 260, 250	354, 689, 709	.431
1.4	67, 189, 142	331, 635, 630	.249
1.6	45, 132	297, 637	.190
1.8	48, 96	321, 641	.150
2.0	37, 91	326, 666	.129
2.2	45, 92	362, 695	.130
2.4	25, 50	313, 652	.078
2.6	17, 51	291, 659	.072
2.8	17, 48	305, 679	.066
3.0	12, 57	311, 712	.067
3.5	10, 31	280, 689	.042
4.0	7, 23	265, 683	.029
4.5	1, 15	264, 652	.017
5.0	0, 5	221, 674	.006
6.0	1, 1	199, 717	.002